

Spin-Orbit Interaction Enabled High-Fidelity Two-Qubit Gates

Jiaan Qi,^{1,*} Zhi-Hai Liu,^{1,†} and H. Q. Xu^{1,2,‡}

¹*Beijing Academy of Quantum Information Sciences, Beijing 100193, China*

²*Beijing Key Laboratory of Quantum Devices, Key Laboratory for the Physics and Chemistry of Nanodevices, and School of Electronics, Peking University, Beijing 100871, China*

We study the implications of spin-orbit interaction (SOI) for two-qubit gates (TQGs) in semiconductor spin qubit platforms. SOI renders the exchange interaction governing qubit pairs anisotropic, posing a serious challenge for conventional TQGs derived for the isotropic Heisenberg exchange. Starting from microscopic level, we develop a concise computational Hamiltonian that captures the essence of SOI, and use it to derive properties of the rotating-frame time evolutions. Two key findings are made. First, for the controlled-phase/controlled-Z gate, we show and analytically prove the existence of “SOI nodes” where the fidelity can be optimally enhanced, with only slight modifications in terms of gate time and local phase corrections. Second, we discover and discuss novel two-qubit dynamics that are inaccessible without SOI—the reflection gate and the direct controlled-not gate. The relevant conditions and achievable fidelities are studied for the direct controlled-not gate.

I. INTRODUCTION

Semiconductor spin qubits are promising candidates for large-scale, fault-tolerant quantum computers due to their potential in industrial scalability and miniaturization in physical size [1]. In this scheme, quantum dots defined in semiconductor devices are commonly used to trap electrons or holes, whose spin states are employed to host quantum information [2]. Currently, high-speed and precise manipulation of single-qubit states is dominantly achieved using rf electric signals [3–6]. The underlying principle behind this technique is spin-orbit interaction (SOI), a key mechanism derived from the relativistic Dirac equation and responsible for many novel effects in mesoscopic physics such as the spin Hall effect [7], spin transistors [8], and Majorana states in superconductor-coupled nanowires [9–12].

Strong SOI is desirable for enabling high-speed single-qubit operation [13, 14]. This constitutes one key reason for the recent push for hole spin qubits [5, 15]. The role of SOI and its influence in two-qubit gates (TQGs) are, however, less straightforward: Seminal works on spin-based quantum computing have universally adopted the simplifying assumption that the inter-spin coupling is described by the Heisenberg exchange interaction [16, 17],

$$H_{\text{ex}} = J \mathbf{S}_1 \cdot \mathbf{S}_2,$$

where \mathbf{S}_1 and \mathbf{S}_2 are the spin operators for the first and second qubit, with the exchange energy J characterizing the coupling strength. The Heisenberg exchange interaction is spherically symmetric with respect to the reference frame and works well for systems with negligible SOI. While it has long been understood in condensed matter theory that SOI gives rise to *anisotropic* exchange coupling, possessing only axial symmetry [18–22]. Specially,

the exchange coupling is described by a tensor \mathcal{J} that permits the decomposition

$$H_{\text{ex}} = \mathbf{S}_1 \mathcal{J} \mathbf{S}_2 = J_{\text{iso}} \mathbf{S}_1 \cdot \mathbf{S}_2 + \mathbf{D} \cdot \mathbf{S}_1 \times \mathbf{S}_2 + \mathbf{S}_1 \Gamma \mathbf{S}_2, \quad (1)$$

where J_{iso} is the isotropic exchange energy, \mathbf{D} is the so-called Dzyaloshinskii-Moriya (DM) vector and Γ is a symmetric tensor of rank-1 [19, 23]. The (last two) anisotropic components of exchange coupling in Eq. (1) is typically small in bulk materials [18], but could be well-comparable to the isotropic part in low-dimensional semiconductor structures [19, 21]. This discrepancy should not be dismissed lightly, for high-fidelity multiple-qubit gates are fundamental to fault-tolerant quantum computing [24–26]. As manufacturing capability evolves, the prospect of an unknown and uncontrolled fidelity loss due to SOI is increasingly relevant and demands urgently for a clear understanding and practical treatment for it.

Much research interest has been drawn to the issue of SOI/anisotropy in recent years. One primary perspective considers the deviation to the Heisenberg exchange as an apparent source of error in TQGs. Various schemes to alleviate the “anisotropy error” have been proposed, typically involving tailoring the control pulses and/or the parameters of the exchange interaction [27–33]. An alternative perspective is to accept the inevitability of anisotropic exchange and build new sets of TQGs that intrinsically accounts for its effects [34–37]. Both of these treatments require extra resources to account for SOI. These overheads increase system complexity and may introduce additional control errors by themselves. A perhaps more fundamental approach to the issue starts from a microscopic description of the SOI, bypassing the phenomenological expressions like Eq. (1). Such studies combining SOI and quantum computing have been carried out for single-electron driving in double-dot [38], spin transport in the presence of SOI [39, 40]. Notably, recent works on microwave-driving controlled-rotation gates on silicon hole spin qubits have revealed SOI sweet-spot in suppressing leakage errors while allowing fast operation frequency [41, 42].

* qija@baqis.ac.cn

† liuzh@baqis.ac.cn

‡ hqxu@pku.edu.cn

In this paper, we present a simple yet generally applicable solution to the SOI issue in TQGs with direct-current (DC) control [43], hopefully clearing the mist of SOI-lead anisotropy. Our paper invites SOI as a key control and optimization parameter in TQGs. This is practically feasible since the SOI coupling strength can be electronically controlled by tuning the gate voltage [44] to a suitably large strength [45]. In Section II, we derive a concise computational Hamiltonian from microscopic theory and show that it is bidirectionally consistent with the phenomenological description of the anisotropic exchange coupling. In Section III, we consider the controlled-phase (CPhase) gates in the presence of SOI. It is shown that with modified local phase corrections, SOI enables direct high-fidelity implementation of the gate, with optimal fidelity achieved on particular SOI nodes. In Section IV, we demonstrate that novel SOI-enabled high-fidelity gates, such as the reflection gate and the direct controlled-not (CNOT) gate have become possible under SOI. Our work suggest new possibilities by proper utilization of SOI. and we hope it could be relevant in the future design of spin qubit systems.

II. THE SOI HAMILTONIAN AND ANISOTROPIC EXCHANGE

Our physical model is a spin-qubit quantum device defined in a semiconductor nanostructure with strong SOI. The detailed structure of the device could be a nanowire or a two-dimensional dot array. To implement joint evolution of neighboring spin pairs, we isolate on a double-quantum-dot (DQD) subsystem from other spins by applying electrostatic confinement, such that electron motion is permit only in the direction along the two dots. For illustrative purpose, we consider a nanowire DQD example in Fig. 1, where a set of barrier and plunger gates is employed to define a double-dot potential $V(x)$ with minima located at $x = \pm d$. The DQD is maintained in a low-energy, half-filling state (containing two electrons only) and subject to a static and possibly inhomogeneous magnetic field $\mathbf{B}(\mathbf{r})$. Some physically achievable constraints are placed to the system. First, the dot separation should be large enough $d > x_0$ such that the orbital states are well-localized. Here, $x_0 \equiv \sqrt{\hbar/m_e^* \Omega}$ is the Bohr radius of the local dot potentials of characteristic frequency Ω and m_e^* is the electron effective mass. Second, the characteristic barrier height $V_0 \gg \hbar\Omega$ should allow multiple bounded orbits in each dot. Finally, the orbital energy $\hbar\Omega$ prevails over the Zeeman energy E_Z and the detuning $\varepsilon \equiv V(-d) - V(d)$.

In general, SOI can consist of the Rashba and the Dresselhaus terms. For the quasi-one-dimensional geometry, the coupling Hamiltonian takes on a simple form: $H_{\text{SO}} = \alpha p_x \sigma_c$, with coupling strength α and the Pauli operator $\sigma_c = \hat{\mathbf{c}} \cdot \boldsymbol{\sigma}$ defined along a vector $\hat{\mathbf{c}}$ uniquely determined by SOI. Presence of SOI modifies many defining aspects of the spin qubit [14]. The spin direction is recog-

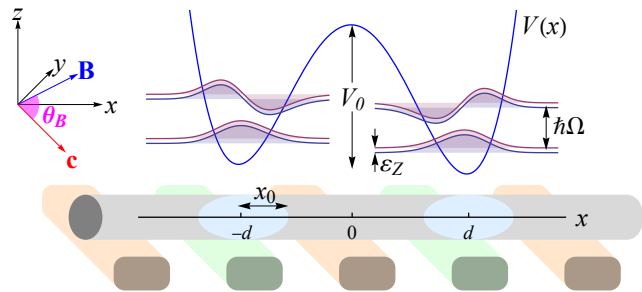


FIG. 1. Schematic illustration of a model two-spin qubit device defined in, e.g., a semiconductor nanowire with strong SOI via a finger-gate technique. The electrostatic potential profile (in blue) and the first 8 low-lying single-electron states staggered by their energy levels are illustrated on top. The top-left inset shows the reference frame and the angle θ_B defined between magnetic field \mathbf{B} and the SOI vector \mathbf{c} .

nized in the “spin frame” $(\hat{\mathbf{a}}, \hat{\mathbf{b}}, \hat{\mathbf{c}})$, defined by placing the magnetic field \mathbf{B} in the upper $\hat{\mathbf{c}}-\hat{\mathbf{a}}$ plane with angle θ_B to the $\hat{\mathbf{c}}$ -axis. The quantization energy reduces from the bare Zeeman energy $E_Z \equiv g\mu_B|\mathbf{B}|$ (g being the Langé-g factor and μ_B the Borh magneton) to $\varepsilon_Z = f_{\text{SO}}E_Z$, for $f_{\text{SO}} \equiv \sqrt{\cos^2 \theta_B + e^{-2(x_0/x_{\text{SO}})^2} \sin^2 \theta_B}$. The qubit states also become entangled in spin and orbital parts,

$$\begin{aligned} |\phi_{\uparrow}\rangle &\simeq \cos(\vartheta/2) |0_+\rangle |\uparrow\rangle + \sin(\vartheta/2) |0_-\rangle |\downarrow\rangle, \\ |\phi_{\downarrow}\rangle &\simeq \cos(\vartheta/2) |0_-\rangle |\downarrow\rangle - \sin(\vartheta/2) |0_+\rangle |\downarrow\rangle, \end{aligned} \quad (2)$$

where $|0_{\pm}\rangle \equiv e^{\pm i\hat{x}/x_{\text{SO}}} |0\rangle$ are the momentum-displaced orbital ground states, with the spin-orbit length $x_{\text{SO}} = \hbar/m_e^* \alpha$, and the mixing angle $\vartheta \equiv \arccos(\cos \theta_B / f_{\text{SO}})$.

One can apply the Hund-Mülliken theory to derive the low-energy Hamiltonian of the DQD system [23]. Linear combination of states (2) at each local dot leads to an energetically-truncated basis $|\Phi_{L\downarrow}\rangle, |\Phi_{L\uparrow}\rangle, |\Phi_{R\downarrow}\rangle, |\Phi_{R\uparrow}\rangle$, where the subscript L/R indicates state localized to the left/right dot. Using the creation/annihilation operators $a_{j\sigma}^\dagger/a_{j\sigma}$ for the state $|\Phi_{j=L,R,\sigma=\uparrow,\downarrow}\rangle$, we can write the Hamiltonian as a sum of the dot term $H_d = \sum_j (\varepsilon_j + \varepsilon_{Z,j}) n_{j\uparrow} + (\varepsilon_j - \varepsilon_{Z,j}) n_{j\downarrow}$, the tunnelling term $H_t = \sum_{\sigma} (t_{\sigma\sigma} a_{L\sigma}^\dagger a_{R\sigma} + t_{\sigma\bar{\sigma}} a_{L\sigma}^\dagger a_{R\bar{\sigma}} + h.c.)$ and the Coulomb term $H_C = \frac{1}{2} U \sum_{j,\sigma} n_{j\sigma} n_{j\bar{\sigma}}$, with $n_{j\sigma} \equiv a_{j,\sigma}^\dagger a_{j,\sigma}$, the on-site energy $\varepsilon_{L/R} = \pm \varepsilon/2$, the charging energy U , and the spin-dependent tunneling coefficients $t_{\sigma\sigma}$ and $t_{\sigma\bar{\sigma}}$. A key insight is that the tunneling coefficients are inter-related in terms of ϑ and the relative SOI strength $\gamma_{\text{SO}} \equiv 2d/x_{\text{SO}}$,

$$\begin{aligned} t_{\downarrow\downarrow} &= t_{\uparrow\uparrow}^* = t_0 (\cos \gamma_{\text{SO}} - i \sin \gamma_{\text{SO}} \cos \vartheta) \equiv t, \\ t_{\downarrow\uparrow} &= t_{\uparrow\downarrow} = t_0 (-i \sin \gamma_{\text{SO}} \sin \vartheta) \equiv s. \end{aligned} \quad (3)$$

Here the spin-conserved (t) and spin-flipped (s) tunneling coefficients are expressed in terms of $t_0 = \sqrt{|t|^2 + |s|^2}$, a common factor that only depends on the interdot spacing d , potential detuning ε and the barrier height V_0 . No particular detail of the potential is otherwise required.

The quantum computational basis comprises the two-electron states $\{|\uparrow\uparrow\rangle, |\uparrow\downarrow\rangle, |\downarrow\uparrow\rangle, |\downarrow\downarrow\rangle\}$, which are the anti-symmetric, half-filling combinations of the single-electron basis states. Higher-energy two-electron states $|S(2, 0)\rangle$ and $|S(0, 2)\rangle$ have non-trivial influence on the $(1, 1)$ subspace through virtual tunneling. Their effects can be kept to $O((t_0/U)^4)$ via a transformation. Combing Eq. (3), we can eventually deduce the effective Hamiltonian for our spin-orbit coupled DQD system as,

$$H = H_0 - J|\xi\rangle\langle\xi|. \quad (4)$$

Here $H_0 \hat{=} \text{diag}(\varepsilon_Z, \frac{1}{2}\delta\varepsilon_Z, -\frac{1}{2}\delta\varepsilon_Z, -\varepsilon_Z)$ defines the qubit quantization energies, with the average and difference Zeeman energy $\varepsilon_Z \equiv (\varepsilon_{Z,L} + \varepsilon_{Z,R})/2$ and $\delta\varepsilon_Z \equiv \varepsilon_{Z,L} - \varepsilon_{Z,R}$. The coupling part is specified by the exchange energy $J \equiv 2t_0^2(\frac{1}{U-\varepsilon} + \frac{1}{U+\varepsilon})$ and an entangled state

$$|\xi\rangle \equiv (s^*|\uparrow\uparrow\rangle + t^*|\uparrow\downarrow\rangle - t|\downarrow\uparrow\rangle + s|\downarrow\downarrow\rangle)/(t_0\sqrt{2}), \quad (5)$$

or alternately $|\xi\rangle \propto |\uparrow\rangle|\nearrow\rangle - |\downarrow\rangle|\swarrow\rangle$ by introducing a pair of “precessed” states $|\nearrow\rangle$ and $|\swarrow\rangle$ from the above. Detailed derivation steps to the above are available in Appendix A.

To verify that our computational Hamiltonian indeed gives rise to the anisotropic exchange coupling, we expand Eq. (4) under the Pauli basis, $H = \mathbf{S}_L \cdot \mathbf{B}_L + \mathbf{S}_R \cdot \mathbf{B}_R + \mathbf{S}_L \cdot \mathcal{J} \mathbf{S}_R$, with the local spin operators $\mathbf{S}_{L/R} = \frac{1}{2}\boldsymbol{\sigma}_{L/R}$, effective magnetic fields $\mathbf{B}_{L/R}$ and the exchange tensor \mathcal{J} . In absence of SOI, \mathcal{J} is just a scalar, recovering the conventional Heisenberg exchange. With nontrivial SOI, \mathcal{J} turns anisotropic. Performing spherical tensor decomposition, we recover the form in Eq. (1), with

$$\begin{aligned} J_0 &= J \cos 2\gamma_{\text{SO}}, \\ \mathbf{D} &= J \sin 2\gamma_{\text{SO}} \hat{\mathbf{v}}, \\ \Gamma &= J 2 \sin^2 \gamma_{\text{SO}} \hat{\mathbf{v}} \hat{\mathbf{v}}, \end{aligned} \quad (6)$$

for the vector $\hat{\mathbf{v}} = (-\sin \vartheta, 0, \cos \vartheta)$. These expressions are consistent with literatures on anisotropic exchange (e.g., Ref. 19). It is quite remarkable that just a single state $|\xi\rangle$ encodes all information required for the dynamics. On the other hand, compared with Eq. (1), the computational Hamiltonian Eq. (4), combined with the state Eq. (5) makes study of TQGs much easier.

III. SOI-ENABLED HIGH-FIDELITY GATES

A. Rotating frame and local phase corrections

Equipped with the computational-space Hamiltonian, we are now well-poised to study the time-evolution of qubit pairs. But before delving into details, we need to clarify issues regarding to the rotating frame and local phase corrections.

Quantum gates are active transformations on quantum states. Ideally, a quantum state should remain

static when the control Hamiltonian is turned off. While an “intrinsic” Hamiltonian H_0 responsible for the qubit quantization energies generates a common passive rotation $R(\tau)$ of quantum states. To offset this effect, quantum states are typically defined in the rotating frame by applying a reverse rotation to the lab-frame states $|\psi(\tau)\rangle_{\text{rf}} = R^{-1}|\psi(\tau)\rangle_{\text{lab}}$ [17]. Naturally, all quantum gates should be understood in this frame. Splitting the total Hamiltonian into $H = H_0 + H_1$, the interaction-picture Hamiltonian $\tilde{H}(\tau) = R^{-1}(\tau)H_1R(\tau)$ is responsible for generating the quantum gate through $\tilde{U}(\tau) = \mathcal{T} \exp\left(-i \int_0^\tau \tilde{H}(\tau') d\tau'\right)$, where \mathcal{T} is the time ordering operator. The exact Dyson series is typically difficult to solve. Alternatively, we can reversely rotate the lab-frame time evolution operator $U(t)$ and get

$$\tilde{U}(\tau) = R^{-1}(\tau)U(\tau) = e^{iH_0\tau}e^{-i(H_0+H_1)\tau}, \quad (7)$$

where we have assumed time-independent Hamiltonian within the time frame involved for the matrix exponential expression. In general $e^{iH_0\tau}e^{-i(H_0+H_1)\tau} \neq e^{-iH_1\tau}$. Particularly when τ is large, both sides are not even close, as the relevant Baker–Campbell–Hausdorff series no longer converges. Dramatic simplification is required for studying properties of $\tilde{U}(\tau)$, which we will show is possible for our effective Hamiltonian in Eq. (4).

The issue of local phase corrections arises mainly from technical perspectives: It is often difficult to directly realize the target gate from the time evolution. Instead, experimentalists may allow any gate that differs from the target gate by local phase gates, $Z_\phi \equiv e^{-i(\phi/2)\sigma_z}$ [16, 46]. Moreover, as is with all quantum states, there can be an arbitrary global phase factor as well. Taking these phase degrees of freedom into account, we define

$$G[\phi] \equiv \{e^{i\phi_0} (Z_{\phi_1} \otimes Z_{\phi_2}) G \mid \forall \phi_0, \phi_1, \phi_2\}. \quad (8)$$

Now the target is not a single point in the $\text{SU}(4)$ space, but rather a three-dimensional manifold charted by the phase parameters (ϕ_0, ϕ_1, ϕ_2) . By turning on a predetermined coupling Hamiltonian, the rotating-frame evolution operator $\tilde{U}(\tau)$ would come across the target manifold $G[\phi]$ at a certain time τ_G . This produces the target gate G when combined with local phase corrections on individual qubits after the transformation, as shown by the circuit model in Fig. 2(a). The justification for introducing local phase gates is that that these single qubit Z -axis rotations can be “virtual” and need not be actually performed [47]. One can completely eliminate these local phase gates by permuting them towards the start or the end of the circuit, or by shifting the microwave phases for single qubit X/Y drives. Despite the apparent freedom in local phases, we should point out that *knowledge* of their values is still important, e.g., at the circuit compilation step, for they can affect final measurement outcomes. Consider for example the circuit in Fig. 2(b), where the upper and lower line represents the control and target qubit and H is the Hadamard gate.

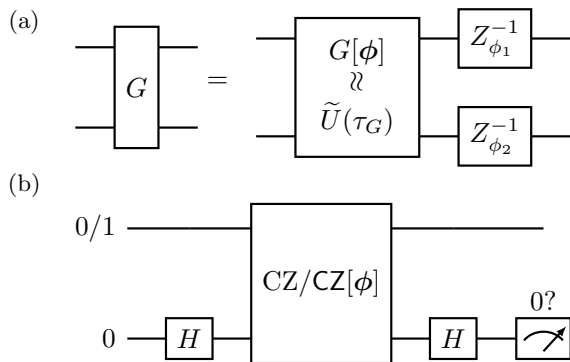


FIG. 2. (a) The circuit implementation of a generic TQG G with local phase freedom. (b) The circuit to determine local phases of an uncorrected CZ gate.

For standard CZ, the circuit outputs state $|00\rangle$ for the input $|00\rangle$ and $|11\rangle$ for input $|10\rangle$. Hence the measurement on the second qubit has full visibility. This is not the case if the CZ gate is replaced with a $\text{CZ}[\phi]$ that has not been phase-corrected, where the possibility for measuring a $|0\rangle$ state on the target qubit would be:

$$P(\text{target} = |0\rangle) = \begin{cases} \cos^2(\phi_2/2), & \text{input} = |00\rangle \\ \sin^2(\phi_2/2), & \text{input} = |10\rangle \end{cases}. \quad (9)$$

We attribute the reduced visibility of the oscillation signals in Ref. 46 to this reason, and this problem is subsequently addressed in Ref. 48. On the other hand, by placing the Hadamard gates on the first line, ϕ_1 can also be measured in a similar fashion. Therefore this circuit setup can be used as a protocol to calibrate the local phase corrections if they are not known in advance.

B. The CPhase/CZ gate

Our first and foremost case study is the CPhase gate, which applies a conditional phase shift to the target qubit. A notable member is the controlled-Z (CZ) gate, a universal TQG defined for controlled π -phase shift. First proposed in Ref. 16 for systems without SOI, the DC implementation of CZ has become the *de facto* way to perform TQGs in state-of-the-art systems [46, 48, 49]. Given its importance, here we exclusively focus on the CZ gate and our results can be extended to the general CPhase gates by simply replacing the π phase with an arbitrary phase of interest.

In the computational basis, CZ is represented as the diagonal matrix $\text{diag}(1, 1, 1, -1)$. Taking account into the local and global phase freedom, we introduce the CZ-class:

$$\text{CZ}[\phi] = e^{i\phi_0} \text{diag}(1, e^{i\phi_2}, e^{i\phi_1}, -e^{i(\phi_1+\phi_2)}), \quad (10)$$

where ϕ_0 is any global phase, $\phi_{1/2}$ is the phase correction required for the first/second qubit. An additional condi-

tions that often appear in literatures is the last diagonal term in Eq. (10) equating 1, where the phase for the parallel states vanishes and one only need to accumulate a combined phase $\phi_1 + \phi_2 = \pi$ for antiparallel states.

To characterize the accuracy of gate implementation, a commonly used indicator is the trace distance function $\frac{1}{2}\|G - G'\|_1$. But here we choose to use is the infidelity between gates, $\text{InF}(G, G') = 1 - \text{Fid}(G, G')$. The infidelity function is mutually bounded with the trace distance and permit easier analysis. For the CZ gate, the instantaneous infidelity function $\text{InF}_{\text{CZ}}(\tau)$ is define by optimizing the infidelity of the time evolution operator $\tilde{U}(\tau)$ to $\text{CZ}[\phi]$ with respect to the phase factors.

$$\text{InF}_{\text{CZ}}(\tau) = \min_{-\pi < \phi_1, \phi_2 \leq \pi} \frac{d^2 - |\text{tr}(\text{CZ}[\phi]^\dagger \tilde{U}(\tau))|^2}{d + d^2}, \quad (11)$$

where the Hilbert space dimension $d = 4$ here. We have restrict the domain since the infidelity function is invariant with respect to global phase and is period in the phase factors. A further optimization with respect to time identifies the CZ gate infidelity, the gate time, and also simultaneously the optimal phase corrections.

$$\text{InF}_{\text{CZ}} \equiv \min_{\tau} \text{InF}_{\text{CZ}}(\tau), \quad \tau_{\text{CZ}} = \arg \min_{\tau} \text{InF}_{\text{CZ}}(\tau)$$

$$(\phi_L, \phi_R) = \arg \min_{\phi_1, \phi_2} \text{InF}_{\text{CZ}}(\tau_{\text{CZ}}).$$

Here we use ϕ_L and ϕ_R to refer to phase corrections on the left and right dot. Additionally, the gate time τ_{CZ} should be restricted to the first period since the function $\text{InF}_{\text{CZ}}(\tau)$ is periodic. In Fig. 3(a), we illustrate the

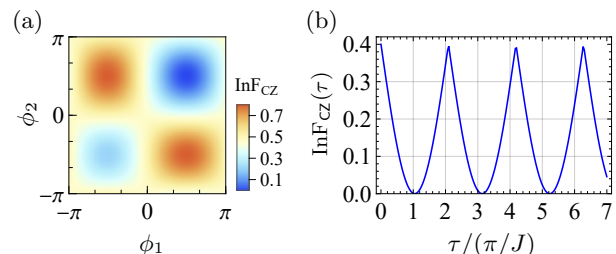


FIG. 3. The infidelity of $\tilde{U}(t)$ to the $\text{CZ}[\phi]$ manifold for a particular energy configuration. (a) The phase-space distribution of the infidelity function at a particular instance $\tau = 0.15\pi/J$. (b) The instantaneous infidelity function $\text{InF}_{\text{CZ}}(\tau)$. The CZ gate is achieved at the infidelity minima around $\tau = 1.05\pi/J$

distribution of the gate infidelity within the phase space (ϕ_L, ϕ_R) at a particular time instance for an example configuration of $\delta E_Z/E_Z = 0.1$, $J/E_Z = 0.02$, $\vartheta = 0.12\pi$ and $\gamma_{\text{SO}} = 0.14\pi$. There can be multiple local minimums in general, and we apply the stochastic differential evolution method to numerically determine the global minimal infidelity at each time instance, yielding the full $\text{InF}_{\text{CZ}}(\tau)$ function in Fig. 3(b). At $\tau_{\text{CZ}} \approx 1.05\pi/J$, $\text{InF}_{\text{CZ}}(\tau)$ is minimized, and the CZ gate is achieved.

One can observe through trying out the numerics that provided $\varepsilon_Z \gg J$, the CZ gate is always attainable with

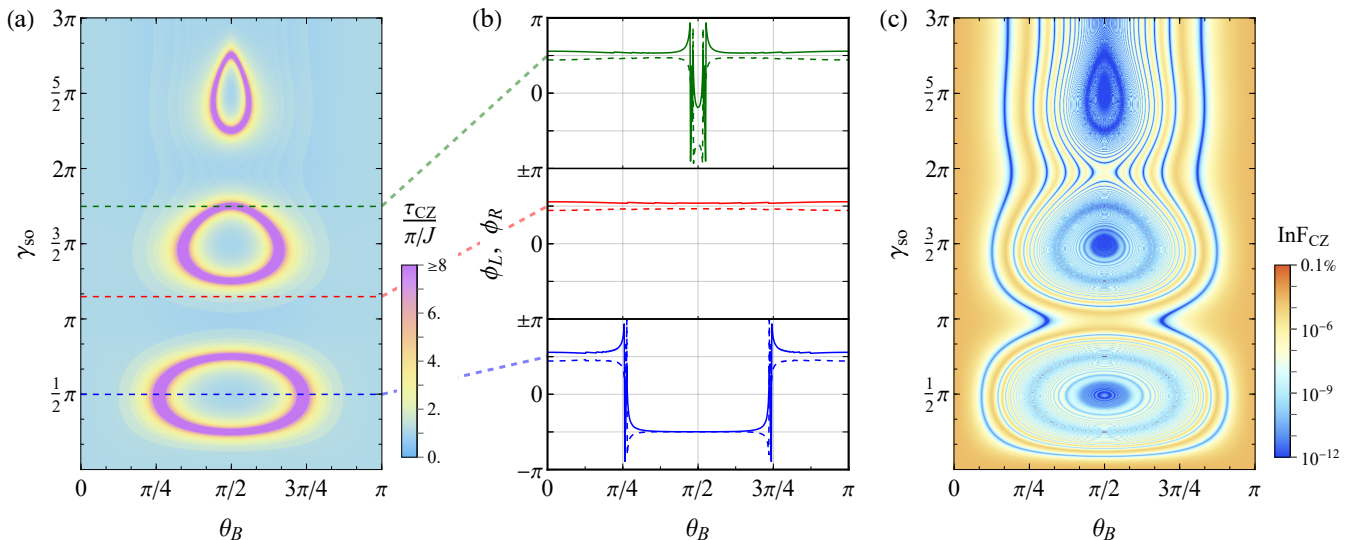


FIG. 4. Parameters of the CZ gate under SOI as functions of the magnetic field angle θ_B and SOI strength γ_{SO} , plotted for a system with $\delta E_Z/E_Z = 0.1$, $J/E_Z = 0.02$ and $d/x_0 = 3$. (a) Gate time τ_{CZ} in unit of π/J . The divergent τ_{CZ} values are truncated at $8\pi/J$, which corresponds to the area with oscillatory local phase corrections. (b) Local phases ϕ_L (solid line) and ϕ_R (dashed line) plotted along the horizontal line cuts in (a), as indicated by their colors and vertical arrangements. (c) Gate infidelity InF_{CZ} in log scale. The case with no SOI corresponds to the $\gamma_{SO} = 0$ line.

high fidelity. But the gate time, local phase corrections and gate infidelity values are subject to the external control and design parameters θ_B and γ_{SO} . Here, we visualize one set of numerical optimization outcomes in Fig. 4 under the settings of $\delta E_Z/E_Z = 0.1$, $J/E_Z = 0.02$ and $d/x_0 = 3$. Fig. 4(a) plots the gate time τ_{CZ} , in which one finds a series of ring-like patterns. The gate time varies slowly around the base value of π/J in most cases but diverges within a relatively small window near the rings. The finite ring width is due to truncation at $8\pi/J$. The choice is made as an indication that on these truncated areas (rings), the CZ gate cannot be robustly carried out due to rapid oscillatory phase values and divergent evolution time. To demonstrate this, we take three constant γ_{SO} lines and plot $\phi_{L/R}$ along these lines in Fig. 4(b). In general, the left and right local phase corrections differ by a small amount and vary slowly near an average value of $\pi/2$ when outside and $-\pi/2$ when inside the rings, but change rapidly right on the rings. Practically, this should not be too concerning though, as one can circumvent these areas by changing θ_B or γ_{SO} . Finally, the gate infidelity InF_{CZ} at τ_{CZ} and optimal $\phi_{L/R}$ is plotted in Fig. 4(c), showing some quite intriguing oscillating patterns. While the most striking feature is that the infidelity inside the rings turns out to be much *lower* than that outside the rings, indicating that the gate quality could be improved by SOI. In particular, one can identify the SOI “nodes” at $\theta_B = \pi/2$ and $\gamma_{SO} = (2k - 1)\pi/2$, ($k = 1, 2, \dots$), i.e., centers of the divergent rings as local minima of the gate infidelity function.

To prove these observation analytically, we consider how the infidelity function can be approximated. Accord-

ing to Eq. (11), only the diagonal elements of $\tilde{U}(\tau)$ enters the calculation of gate infidelity since $\text{CZ}[\phi]$ is diagonal by definition. Assuming $\varepsilon_Z \gg J$, we can determine these diagonal elements with the help of perturbation theory. By assumption, the Hamiltonian $H = H_0 - J|\xi\rangle\langle\xi|$ can be seen as H_0 perturbed by a much smaller term. Let us denote the eigenenergies of H_0 as $E_n^{(0)} \equiv \langle n|H_0|n\rangle$, where $|n\rangle$ is the n th computational basis state. The perturbed eigenenergies and eigenstates are denoted as $E'_n = E_n^{(0)} + \delta E_n$ and $|n'\rangle$. To calculate the diagonal elements of $\tilde{U}(\tau)$, we invoke Eq. (7) and take the matrix exponential $e^{-iH\tau}$ in the eigenstate basis of H and then perform projection onto the diagonal space. Also since H_0 is already diagonal, we have

$$\begin{aligned} \langle n|\tilde{U}(\tau)|n\rangle &= e^{iE_n^{(0)}\tau} \langle n|e^{-iH\tau}|n\rangle \\ &= |\langle n|n'\rangle|^2 e^{-i\delta E_n\tau} + \sum_{m \neq n} |\langle n|m'\rangle|^2 e^{-i(E'_m - E_n^{(0)})\tau}, \end{aligned} \quad (12)$$

where we have split the expression into a summation of a major term ($O(1)$) originating from the same-energy overlap, and multiple minor terms $O((J/\varepsilon_Z)^2)$ originating from correction due to different energy levels. For our goal of deriving a perturbative expression, it suffice to consider the condition where the major part implements $\text{CZ}[\phi]$ and absorb the rest into errors. Comparing with Eq. (10), we see that the DC evolution reaches the target $\text{CZ}[\phi]$ gate when it meet the phase-matching condition:

$$(\delta E_1 + \delta E_4 - \delta E_2 - \delta E_3)\tau = (2k + 1)\pi, \quad k \in \mathbb{Z}. \quad (13)$$

To derive an appropriate condition, we consider the first order energy perturbations $\delta E_n^{(1)} = -J|\langle n|\xi\rangle|^2$. The

phase matches when the evolution time τ becomes odd multiple of

$$\tau_{\text{CZ}} = \frac{\pi/J}{\left| |\tilde{t}|^2 - |\tilde{s}|^2 \right|}, \quad (14)$$

where $\tilde{t} = t/t_0$ and $\tilde{s} = s/t_0$. This expression is still valid after including the second order energy corrections, which cancel out in Eq. (13) due to the symmetric distribution of H_0 eigenvalues. The divergent condition $|t| = |s|$ produces exactly the rings observed in Fig. 4(a). Physically speaking, the CZ gate requires a π -phase difference between the spin-parallel states and the spin-antiparallel states. Yet when $|t| = |s|$, the spin-flipped and spin-conserved tunneling processes are equal in strength, and there is a symmetry in the Hamiltonian between these two sets of states. A phase difference is unable to accumulate thus the divergent gate time.

After explicitly setting the global and local phase factors to satisfy $\phi_0 = -\delta E_1 \tau_{\text{CZ}}$, $\phi_0 + \phi_{\text{R}} = -\delta E_2 \tau_{\text{CZ}}$ and $\phi_0 + \phi_{\text{L}} = -\delta E_3 \tau_{\text{CZ}}$, we have the phase of $\text{diag } \hat{U}_{\text{major}}$ matches that of $\text{CZ}[\phi]$. The corresponding local phase corrections are found to be

$$\begin{aligned} \phi_{\text{L}} \approx \phi_{\text{R}} \approx \frac{\pi}{2}, & \quad \text{when } |\tilde{t}| > |\tilde{s}| \\ \phi_{\text{L}} \approx \phi_{\text{R}} \approx -\frac{\pi}{2}, & \quad \text{when } |\tilde{t}| < |\tilde{s}| \end{aligned} \quad (15)$$

at the first order perturbation. Inclusion of the second order perturbation will produce a difference between the two local phase corrections, as detailed in Appendix B. When the gate time and the local phase corrections are accurately carried out, the resulting time evolution is a high-fidelity implementation of the CZ gate. The gate fidelity is determined by the non-unity norm of the major part in addition to the minor part. As derived in Appendix B, we have the infidelity estimation

$$\text{InF}_{\text{CZ}} \lesssim \frac{1}{10} \left(\frac{J}{\varepsilon_{\text{Z}}} \right)^2 \left[|\tilde{s}|^4 + \frac{4|\tilde{t}|^4}{\delta^2} + \frac{64(4 + \delta^2)}{(4 - \delta^2)^2} |\tilde{s}|^2 |\tilde{t}|^2 \right], \quad (16)$$

where $\delta \equiv \delta \varepsilon_{\text{Z}} / \varepsilon_{\text{Z}}$ is a dimensionless number characterizing the Zeeman field gradient. Our infidelity expression is derived only from the second order eigenenergy and first order eigenstate perturbation, but sufficient to study the qualitative behavior of the full optimization results. In particular, the gate-fidelity is not a monotonous function of the SOI strength. An obvious choice for enhancing gate quality is to find a ‘‘sweet spot’’ where the RHS of Eq. (16) is kept as small as possible. To find the optimal working condition, we define the square-bracketed terms in the infidelity upper bound as κ . Through the relation $|\tilde{s}|^2 + |\tilde{t}|^2 = 1$, we can write κ as a function of $\delta > 0$ and $x \equiv |\tilde{s}|^2 \in [0, 1]$:

$$\kappa = x^2 + \frac{4(1-x)^2}{\delta^2} + \frac{64(\delta^2 + 4)x(1-x)}{(\delta^2 - 4)^2}. \quad (17)$$

After taking the first and second order derivatives with respect to x , we find that κ attains minimum at either $x = 0$ or $x = 1$. Combined with the definition that $\tilde{s} = -i \sin \gamma_{\text{SO}} \sin \vartheta$, This suggests that the gate infidelity achieves minima either when SOI is absent ($\gamma_{\text{SO}} = 0$) or when $\vartheta = \pi/2$ and $\gamma_{\text{SO}} = (k - \frac{1}{2})\pi$, namely, at an SOI node. Explicitly, for the case without SOI, we have

$$\text{InF}_{\text{CZ}}(\gamma_{\text{SO}} = 0) \lesssim \frac{2}{5} \left(\frac{J}{\delta E_{\text{Z}}} \right)^2, \quad (18)$$

where we used the bare Zeeman energy E_{Z} here instead of ε_{Z} since $f_{\text{SO}} = 1$. On the other hand, at the k th SOI node,

$$\begin{aligned} \text{InF}_{\text{CZ}}(\gamma_{\text{SO}} = (k - \frac{1}{2})\pi) & \lesssim \frac{1}{10} \left(\frac{J}{f_{\text{SO}} E_{\text{Z}}} \right)^2 \\ & = \frac{1}{10} \left(\frac{J}{E_{\text{Z}}} \right)^2 \exp \left[\frac{(2k\pi - \pi)^2}{8(d/x_0)^2} \right]. \end{aligned} \quad (19)$$

It appears as if f_{SO} is playing the role of magnetic field gradient δ here.

The implications of Eq. (18) and Eq. (19) are immediate. On one hand, to achieve high fidelity gate in system with negligible SOI, a large interdot difference in the qubit energy is required. Thus, in a system with a small g -factor variation, device design involving large magnetic field gradient δE_{Z} is a theoretical necessity rather than a technical choice. On the other hand, large magnetic field gradient is optional for quantum dots made in a semiconductor nanostructure with large SOI. The fidelity sweet-spot can be attained in systems where the dot geometry matches the SOI strength. In particular, we require

$$4d = \pi x_{\text{SO}}, \quad (20)$$

for the first SOI node. This condition is within reach for practical systems with x_{SO} in the order of 100nm [50].

IV. SOI-ENABLED GATE DYNAMICS

Looking beyond the CPhase gate, other novel two-qubit dynamics is also enabled after adding the SOI ingredient. Here we briefly discuss two such possibilities—the two-qubit reflection gate and the CNOT gate.

It is well-known that evolving the Heisenberg exchange Hamiltonian for $\tau = \pi/J$ [2] produces the SWAP gate, which induces $|\varphi\rangle|\psi\rangle \rightarrow |\psi\rangle|\varphi\rangle$ for all single-qubit states $|\varphi\rangle$ and $|\psi\rangle$. Here, evolving the anisotropic exchange Hamiltonian $H_{\text{ex}} = -J|\xi\rangle\langle\xi|$ leads to

$$e^{-i(\pi/J)H_{\text{ex}}} = \mathbb{I} - 2|\xi\rangle\langle\xi|, \quad (21)$$

i.e., a reflection of the two-qubit Hilbert space with respect to $|\xi\rangle$. The reflection gate generalizes over the SWAP gate. The later can be seen as the state reflection with respect to the Bell state $|\Psi^-\rangle = \frac{1}{\sqrt{2}}(|\uparrow\downarrow\rangle - |\downarrow\uparrow\rangle)$. The reflection gate recovers the SWAP gate for $\gamma_{\text{SO}} = 0$, but

offers more flexible transformations with finite SOI. By adjusting the magnetic field angle and the SOI strength, one can artificially design a large class of state $|\xi\rangle$ that can be used to achieve a single-step reflection. A high-fidelity implementation of the reflection gate is achievable at the large coupling limit $J \gg \varepsilon_Z$ —the opposite to the controlled phase gates. The gate fidelity can be further improved with optimal local phase corrections.

A perhaps more interesting example is the DC implementation of the CNOT gate. Conventionally, the CNOT gate can be implemented in the AC way, i.e., by applying a resonant microwave drive to induce transition between the $|\downarrow\uparrow\rangle$ and $|\downarrow\downarrow\rangle$ states [51]. Compared with the AC approach, the DC gate implementation, if possible, is more preferred as it uses easier static control signals and is less susceptible to charge noise [52]. It would be impossible to attain the CNOT gate by a single-step DC evolution without SOI, as can be proven by showing the commutator $[\text{CNOT}, H(\gamma_{\text{SO}} = 0)] \neq 0$ for finite exchange coupling J . When SOI is present, however, the CNOT gate can be achieved under appropriate conditions. Let us use the rotated basis $\{|\uparrow\nearrow\rangle, |\uparrow\swarrow\rangle, |\downarrow\swarrow\rangle, |\downarrow\nearrow\rangle\}$ for convenience. At the Zeeman splitting condition $E_{Z,L} = 3E_{Z,R}$, the Hamiltonian (4) is represented as

$$H_0 - J|\xi\rangle\langle\xi| \hat{=} \begin{pmatrix} \varepsilon_Z & 0 & 0 & 0 \\ 0 & \varepsilon_Z & 0 & 0 \\ 0 & 0 & \varepsilon_Z & 0 \\ 0 & 0 & 0 & \varepsilon_Z \end{pmatrix} - \begin{pmatrix} \frac{J}{2} & 0 & 0 & \frac{J}{2} \\ 0 & 0 & 0 & 0 \\ 0 & 0 & 0 & 0 \\ \frac{J}{2} & 0 & 0 & \frac{J}{2} \end{pmatrix}. \quad (22)$$

The representation of CNOT is in general not diagonal in this basis—unless if the effective SOI strength is fixed at $\gamma_{\text{SO}} = \pi/2$, we have

$$\begin{aligned} \text{C}_1\text{NOT}_2 &\hat{=} \text{diag}(1, 1, 1, -1) \quad \text{at } \vartheta = \pi/4, \\ \text{C}_2\text{NOT}_1 &\hat{=} \text{diag}(-1, 1, 1, 1) \quad \text{at } \vartheta = 3\pi/4, \end{aligned} \quad (23)$$

where the subscripts for C and NOT represent the control and target qubit. In both cases, they transform trivially in the rotating frame defined by H_0 . Equating the interaction picture evolution $\tilde{U}(\tau) = e^{iH_0\tau} e^{-iH\tau}$ to either CNOT gates, we obtain three independent energy-time constraints:

$$\begin{aligned} J\tau &= (2l+1)\pi, \quad 2\varepsilon_Z\tau = (2m+1)\pi, \\ \sqrt{4\varepsilon_Z^2 + J^2} \tau &= 2n\pi, \quad \text{where } l, m, n \in \mathbb{N}. \end{aligned} \quad (24)$$

If these constraints hold, the CNOT gate can be perfectly achieved (there is no need for local phase corrections). However, just like the CZ gate cannot be perfectly achieved, these three conditions cannot hold simultaneously, since there is no Pythagorean triple satisfying $(2l+1)^2 + (2m+1)^2 = (2n)^2$ [53]. But it suffices to achieve a high-fidelity gate provided that these conditions hold *approximately*. In Fig. 5, we numerically compute the gate fidelity of the C_1NOT_2 and C_2NOT_1 as a function of the dimensionless exchange energy J/ε_Z and evolution time $\varepsilon_Z\tau$ (in units determined by the qubit energy ε_Z).

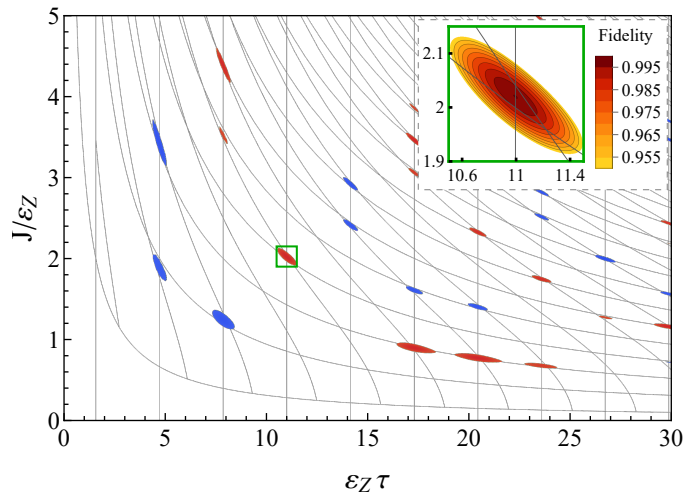


FIG. 5. Numerically computed high fidelity ($> 95\%$) regions of the two-qubit CNOT gate (blue for C_2NOT_1 and red for C_1NOT_2) through DC evolution and conditions described in Eq. (24) (grey lines). The inset shows a zoom-in area where the gate fidelity values are explicitly given.

One can see that the high-fidelity regions appear precisely at the approximate intersections of the constraints in Eqs. (24). Through a suitable combination of the effective SOI strength γ_{SO} , the magnetic field angle θ_B , the exchange energy J and evolution time τ , one can implement the CNOT gate with fidelity surpassing 99.5% by just a single-step evolution. In Table I, we compute and summarize a list of high-fidelity points of the CNOT gate for the range considered in Fig. 5. This could be used for reference in future experimental implementations.

Gate	$\varepsilon_Z\tau$	J/ε_Z	Fidelity
C_2NOT_1	20.4204	4.15737	0.99958
C_1NOT_2	17.2788	3.46028	0.99918
C_2NOT_1	26.7035	1.99654	0.99914
C_1NOT_2	23.5619	4.94016	0.99795
C_1NOT_2	23.5619	4.65948	0.99772
C_1NOT_2	7.85398	4.37725	0.99744
C_1NOT_2	26.7035	3.18416	0.99643
C_1NOT_2	20.4204	0.77555	0.99599
C_1NOT_2	10.9956	2.02033	0.99504
C_1NOT_2	17.2788	0.89983	0.99493

TABLE I. A selected list of high-fidelity solutions of Eq. (24) for the CNOT gate, sorted by the estimated optimal fidelity.

V. CONCLUSIONS

In summary, we have studied the role of SOI in the dynamics of a spin qubit pair. For an exchange-coupled two-electron spin system, the compact computational Hamiltonian of Eq. (4) is derived and the connection of SOI to the anisotropic exchange interaction is revealed.

Using this Hamiltonian, we deliver the central message that SOI needs not be treated as a noise source in TQGs, but rather can be naturally taken as advantages. Specifically, it is shown that the CPhase gate can be accurately implemented with adaption of SOI, and the gate fidelity is optimized at certain practically attainable SOI nodes. It is also shown that SOI enable two-qubit dynamics that are conventionally impossible, with the general reflection gate and the CNOT gate examples explicitly constructed. Finally, we must point out that the dynamics considered here is purely unitary and errors involved are coherent in nature. This simple model should serve to demonstrate the power of SOI for facilitating high-fidelity gates and

for creating novel possibilities in constructing spin-based quantum computing chips.

ACKNOWLEDGMENTS

This work is supported by the Beijing Postdoctoral Research Foundation (Grant No. 2023-zz-050), the National Natural Science Foundation of China (Grant Nos. 92165208 and 11874071) and the Key-Area Research and Development Program of Guangdong Province (Grant No. 2020B0303060001). We would like to thank Ji-Yin Wang and Yi Luo for helpful discussions.

-
- [1] F. P. García de Arquer, D. V. Talapin, V. I. Klimov, Y. Arakawa, M. Bayer, and E. H. Sargent, *Science* **373**, eaaz8541 (2021).
- [2] D. Loss and D. P. DiVincenzo, *Physical Review A* **57**, 120 (1998).
- [3] J. W. G. van den Berg, S. Nadj-Perge, V. S. Pribiag, S. R. Plissard, E. P. A. M. Bakkers, S. M. Frolov, and L. P. Kouwenhoven, *Physical Review Letters* **110**, 066806 (2013).
- [4] J. Yoneda, K. Takeda, T. Otsuka, T. Nakajima, M. R. Delbecq, G. Allison, T. Honda, T. Kodera, S. Oda, Y. Hoshi, N. Usami, K. M. Itoh, and S. Tarucha, *Nature Nanotechnology* **13**, 102 (2018).
- [5] F. N. M. Froning, L. C. Camenzind, O. A. H. van der Molen, A. Li, E. P. A. M. Bakkers, D. M. Zumbühl, and F. R. Braakman, *Nature Nanotechnology* **16**, 308 (2021).
- [6] A. Mills, C. Guinn, M. Feldman, A. Sigillito, M. Gullans, M. Rakher, J. Kerckhoff, C. Jackson, and J. Petta, *Physical Review Applied* **18**, 064028 (2022).
- [7] Y. K. Kato, R. C. Myers, A. C. Gossard, and D. D. Awschalom, *Science* **306**, 1910 (2004).
- [8] S. D. Sarma, *Rev. Mod. Phys.* **76**, 88 (2004).
- [9] J. D. Sau, R. M. Lutchyn, S. Tewari, and S. Das Sarma, *Physical Review Letters* **104**, 040502 (2010).
- [10] Y. Oreg, G. Refael, and F. von Oppen, *Physical Review Letters* **105**, 177002 (2010).
- [11] V. Mourik, K. Zuo, S. M. Frolov, S. R. Plissard, E. P. A. M. Bakkers, and L. P. Kouwenhoven, *Science* **336**, 1003 (2012).
- [12] M. T. Deng, C. L. Yu, G. Y. Huang, M. Larsson, P. Caroff, and H. Q. Xu, *Nano Letters* **12**, 6414 (2012).
- [13] V. N. Golovach, M. Borhani, and D. Loss, *Physical Review B* **74**, 165319 (2006).
- [14] R. Li, J. Q. You, C. P. Sun, and F. Nori, *Physical Review Letters* **111**, 086805 (2013).
- [15] H. Watzinger, J. Kukučka, L. Vukušić, F. Gao, T. Wang, F. Schäffler, J.-J. Zhang, and G. Katsaros, *Nature Communications* **9**, 3902 (2018).
- [16] T. Meunier, V. E. Calado, and L. M. K. Vandersypen, *Physical Review B* **83**, 121403 (2011).
- [17] M. Russ, D. M. Zajac, A. J. Sigillito, F. Borjans, J. M. Taylor, J. R. Petta, and G. Burkard, *Physical Review B* **97**, 085421 (2018).
- [18] K. V. Kavokin, *Physical Review B* **64**, 075305 (2001).
- [19] K. V. Kavokin, *Physical Review B* **69**, 075302 (2004).
- [20] D. Stepanenko, N. E. Bonesteel, D. P. DiVincenzo, G. Burkard, and D. Loss, *Physical Review B* **68**, 115306 (2003).
- [21] F. Baruffa, P. Stano, and J. Fabian, *Physical Review Letters* **104**, 126401 (2010); *Physical Review B* **82**, 045311 (2010).
- [22] R. Li and J. Q. You, *Physical Review B* **90**, 035303 (2014).
- [23] Z.-H. Liu, O. Entin-Wohlman, A. Aharony, and J. Q. You, *Physical Review B* **98**, 241303 (2018).
- [24] E. Knill, R. Laflamme, and W. H. Zurek, *Proceedings of the Royal Society of London. Series A: Mathematical, Physical and Engineering Sciences* **454**, 365 (1998).
- [25] D. Aharonov and M. Ben-Or, *SIAM Journal on Computing* **38**, 1207 (2008).
- [26] X. Xue, M. Russ, N. Samkharadze, B. Undseth, A. Sammak, G. Scappucci, and L. M. K. Vandersypen, *Nature* **601**, 343 (2022).
- [27] N. E. Bonesteel, D. Stepanenko, and D. P. DiVincenzo, *Physical Review Letters* **87**, 207901 (2001).
- [28] G. Burkard and D. Loss, *Physical Review Letters* **88**, 047903 (2002).
- [29] X. Hao and S. Zhu, *Physical Review A* **76**, 044306 (2007).
- [30] G.-F. Zhang and Y. Zhou, *Physics Letters A* **370**, 136 (2007).
- [31] X. Hao and S. Zhu, *Physics Letters A* **372**, 1119 (2008).
- [32] R. J. Guerrero and F. Rojas, *Physical Review A* **77**, 012331 (2008).
- [33] Y. Zhou and G.-F. Zhang, *Optics Communications* **316**, 22 (2014).
- [34] L.-A. Wu and D. A. Lidar, *Physical Review A* **66**, 062314 (2002).
- [35] D. Stepanenko and N. E. Bonesteel, *Physical Review Letters* **93**, 140501 (2004).
- [36] C. Flindt, A. S. Sørensen, and K. Flensberg, *Physical Review Letters* **97**, 240501 (2006).
- [37] M. Milivojević and D. Stepanenko, *Journal of Physics: Condensed Matter* **29**, 405302 (2017); M. Milivojević, *Journal of Physics: Condensed Matter* **30**, 085302 (2018).
- [38] D. V. Khomitsky, L. V. Gulyaev, and E. Ya. Sherman, *Physical Review B* **85**, 125312 (2012).
- [39] Y.-C. Li, X. Chen, J. G. Muga, and E. Y. Sherman, *New Journal of Physics* **20**, 113029 (2018).
- [40] X. Zhao and X. Hu, *Scientific Reports* **8**, 13968 (2018).

- [41] S. Geyer, B. Hetényi, S. Bosco, L. C. Camenzind, R. S. Eggli, A. Fuhrer, D. Loss, R. J. Warburton, D. M. Zumbühl, and A. V. Kuhlmann, Two-qubit logic with anisotropic exchange in a fin field-effect transistor (2022), [arxiv:2212.02308](#) [cond-mat, physics:quant-ph].
- [42] M. Spethmann, S. Bosco, A. Hofmann, J. Klinovaja, and D. Loss, High-fidelity two-qubit gates of hybrid superconducting-semiconducting singlet-triplet qubits (2023), [arxiv:2304.05086](#) [cond-mat, physics:quant-ph].
- [43] By DC control, we refer to the time evolution where the Hamiltonian is static in time.
- [44] J. Nitta, T. Akazaki, H. Takayanagi, and T. Enoki, *Physical Review Letters* **78**, 1335 (1997).
- [45] S. Bosco, B. Hetényi, and D. Loss, *PRX Quantum* **2**, 010348 (2021).
- [46] M. Veldhorst, C. H. Yang, J. C. C. Hwang, W. Huang, J. P. Dehollain, J. T. Muhonen, S. Simmons, A. Laucht, F. E. Hudson, K. M. Itoh, A. Morello, and A. S. Dzurak, *Nature* **526**, 410 (2015).
- [47] L. M. K. Vandersypen, *Rev. Mod. Phys.* **76**, 33 (2004).
- [48] T. F. Watson, S. G. J. Philips, E. Kawakami, D. R. Ward, P. Scarlino, M. Veldhorst, D. E. Savage, M. G. Lagally, M. Friesen, S. N. Coppersmith, M. A. Eriksson, and L. M. K. Vandersypen, *Nature* **555**, 633 (2018).
- [49] K. Takeda, A. Noiri, T. Nakajima, T. Kobayashi, and S. Tarucha, *Nature* **608**, 682 (2022).
- [50] J.-Y. Wang, G.-Y. Huang, S. Huang, J. Xue, D. Pan, J. Zhao, and H. Xu, *Nano Letters* **18**, 4741 (2018).
- [51] D. M. Zajac, A. J. Sigillito, M. Russ, F. Borjans, J. M. Taylor, G. Burkard, and J. R. Petta, *Science* **359**, 439 (2018).
- [52] M. Rimbach-Russ, S. G. J. Philips, X. Xue, and L. M. K. Vandersypen, Simple framework for systematic high-fidelity gate operations (2022), [arxiv:2211.16241](#) [cond-mat, physics:quant-ph].
- [53] J. H. Silverman, *A Friendly Introduction to Number Theory*, 4th ed. (Pearson, Boston, 2012) Chap. 2.

Appendix A: Deriving the computational Hamiltonian

1. Frame setup and problem outline

In general, we can write the total Hamiltonian as a sum of the single-electron Hamiltonian and electron-electron interaction Hamiltonian,

$$H = \sum_{i=1,2} H_e(\mathbf{r}_i) + \frac{e^2}{4\pi\epsilon_e|\mathbf{r}_1 - \mathbf{r}_2|}, \quad (\text{A1})$$

where ϵ_e is the electric permittivity of the device. H_e consists of

$$H_e(\mathbf{r}) = \frac{\mathbf{p}^2}{2m_e^*} + V(\mathbf{r}) + H_{\text{SO}} + H_Z, \quad (\text{A2})$$

where H_{SO} is the SOI Hamiltonian and H_Z is the Zeeman Hamiltonian. The momentum operator is given by $\mathbf{p} = -i\hbar\nabla + e\mathbf{A}$ under the magnetic field $\mathbf{B}(\mathbf{r}) = \nabla \times \mathbf{A}$. We leave out the optional rf electric field term here as it is irrelevant for our DC TQG implementations.

The SOI in a semiconductor can in general consists of the Rashba and Dresselhaus terms as a result of bulk inversion asymmetry and structural inversion asymmetry. The forms of interaction are normally defined in the crystallographic frame. By choosing $\hat{\mathbf{x}}' \parallel [100]$, $\hat{\mathbf{y}}' \parallel [010]$, $\hat{\mathbf{z}}' \parallel [001]$, and assuming that the device is fabricated in the (001) plane, we have, $H_{\text{SO}} = \alpha_R (p_{x'}\sigma_{y'} - p_{y'}\sigma_{x'}) + \alpha_D (p_{x'}\sigma_{x'} - p_{y'}\sigma_{y'})$, where α_R and α_D are the coupling strengths for the Rashba and Dresselhaus effects respectively. For our DQD system, the electron motion is further restricted to quasi-one-dimension along the dots. This defines the “device frame” $(\hat{\mathbf{x}}, \hat{\mathbf{y}}, \hat{\mathbf{z}})$, where the quantum dots are lining along the $\hat{\mathbf{x}}$ axis and $\hat{\mathbf{z}} \parallel \hat{\mathbf{z}}'$. Denoting the angle between $\hat{\mathbf{x}}$ and $\hat{\mathbf{x}}'$ as $\varphi_{xx'}$, we can derive, for our DQD system,

$$\begin{aligned} H_{\text{SO}} &= p_x (\alpha_R \sigma_y + \alpha_D \cos 2\varphi_{xx'} \sigma_x - \alpha_D \sin 2\varphi_{xx'} \sigma_y) \\ &= p_x (\alpha \hat{\mathbf{c}} \cdot \boldsymbol{\sigma}) = \alpha p_x \sigma_c, \end{aligned} \quad (\text{A3})$$

where $\hat{\mathbf{c}} \equiv \alpha^{-1}(\alpha_D \cos 2\varphi_{xx'} \hat{\mathbf{x}} + (\alpha_R - \alpha_D \sin 2\varphi_{xx'}) \hat{\mathbf{y}})$ is a unit vector representing the direction of SOI and α is the normalized SOI coupling coefficient. The restriction to one-dimension also suppresses cyclotron movement of electrons and we can neglect the gauge field \mathbf{A} as well.

Despite restriction in electron orbital motion, the electron spin can still point to all directions. For systems with strong SOI, spin is more conveniently represented in the “spin frame”— $(\hat{\mathbf{a}}, \hat{\mathbf{b}}, \hat{\mathbf{c}})$ —with spin-up/down along the $\pm\hat{\mathbf{c}}$ direction. To eliminate the remaining uncertainty in $\hat{\mathbf{a}}$ and $\hat{\mathbf{b}}$, we demand that the magnetic field \mathbf{B} lying in the upper $\hat{\mathbf{c}}-\hat{\mathbf{a}}$ plane, such that $\theta_B \in [0, \pi]$ denotes the angle between \mathbf{B} and $\hat{\mathbf{c}}$. Naturally, $\hat{\mathbf{b}} = \hat{\mathbf{c}} \times \hat{\mathbf{a}}$, and we can identify

$$H_Z = \frac{1}{2} E_Z(\mathbf{r}) (\cos \theta_B \sigma_c + \sin \theta_B \sigma_a), \quad (\text{A4})$$

where $E_Z \equiv g(\mathbf{r})\mu_B|\mathbf{B}(\mathbf{r})|$ is the Zeeman splitting energy, with $g(\mathbf{r})$ being the position-dependent Landé-g factor and μ_B the Bohr magneton.

The positional basis used in Eq. (A1) to Eq. (A4) is inconvenient for studying the low energy dynamics of the system since the representation is uncountably-infinite dimensional. A much better choice is the single-electron energy eigenstates, where H_e is diagonal and we can truncate the basis to the first few terms to write down the low energy Hamiltonian. This scheme is all good except it is hard to find the exact eigenstates. Instead, another orthonormal set of electron wave function $\{|\Phi_\mu\rangle\}$ can be used. Notice $|\Phi_\mu\rangle$ need not be a product state of the orbital and the spin wave functions. As long as the low energy eigenstates resides in the span of the first few terms of the basis, we may truncate the basis to obtain a matrix of a finite dimension. Hence the goal now is to find an appropriate basis to support the low energy wave functions. For our DQD system, we can construct a basis by the ‘‘linear combination of atomic orbits’’ method by first solving for the wave functions for two single dots and then linearly combining the two local dot wave functions to form a DQD basis.

2. The single-dot problem

Suppose we have a single dot subject to harmonic local potential at the center of the coordinate system. Its static Hamiltonian can be written under the effective mass approximation as

$$H_{\text{sd}} = \frac{p^2}{2m_e^*} + \frac{1}{2}m_e^*\Omega^2x^2 + H_{\text{so}} + H_Z \quad (\text{A5})$$

Even for such simple potential profile, analytical solutions cannot be found in a closed form. Writing down its eigenenergies and eigenstates would still require perturbation theory. Formal treatment of such Hamiltonian can be found in, e.g., Ref. 13 and Ref. 14. We will follow the latter approach here, which uses the Zeeman term as perturbation, allowing treatment of strong SOI.

First, we define the unperturbed Hamiltonian H_0 as the H_{sd} in Eq. (A5) excluding H_Z . Conjugating H_0 with $e^{i(x/x_{\text{SO}})\sigma_c}$ yields, up to a constant, the simple harmonic oscillator Hamiltonian. Therefore the H_0 eigenvalues and eigenstates are found to be

$$E_{n\sigma}^{(0)} = \hbar\Omega(n + \frac{1}{2}) - \frac{1}{2}m_e^*\alpha^2, \quad (\text{A6})$$

$$|\phi_{n\sigma}^{(0)}\rangle = e^{-is_\sigma x/x_{\text{SO}}}|n\rangle|\sigma\rangle \text{ with } \sigma \in \{\uparrow, \downarrow\}, \quad (\text{A7})$$

where $|n\rangle$ is the n th harmonic oscillator eigenstate, and $s_{\uparrow\downarrow} = \pm 1$ is the spin-sign function. It is seen that for H_0 , states with same orbital number n and opposite spins are degenerate. This degeneracy is lifted by turning on H_Z . The degenerate perturbation theory requires finding an appropriate basis that diagonalizes H_Z . For the orbital ground states in particular,

$$\langle 0|H_Z|0\rangle = \frac{E_Z}{2} \begin{pmatrix} \cos\theta_B & e^{-(\frac{x_0}{x_{\text{SO}}})^2} \sin\theta_B \\ e^{-(\frac{x_0}{x_{\text{SO}}})^2} \sin\theta_B & -\cos\theta_B \end{pmatrix}. \quad (\text{A8})$$

Diagonalizing this matrix, we find the first-order energy corrections and the suitably oriented eigenstates to be

$$E_{0\sigma}^{(1)} = s_\sigma \frac{1}{2} f_{\text{so}} E_Z \equiv s_\sigma \frac{1}{2} \varepsilon_Z, \quad (\text{A9})$$

$$|\phi_{0\sigma}^{(0')}\rangle = \cos(\frac{\vartheta}{2}) |\phi_{0\sigma}^{(0)}\rangle + s_\sigma \sin(\frac{\vartheta}{2}) |\phi_{0\bar{\sigma}}^{(0)}\rangle, \quad (\text{A10})$$

where we have defined the SOI-related factors

$$f_{\text{so}} \equiv \sqrt{\cos^2\theta_B + e^{-2\eta_{\text{so}}^2} \sin^2\theta_B}, \quad (\text{A11})$$

$$\vartheta \equiv \arccos(\cos\theta_B/f_{\text{so}}), \quad (\text{A12})$$

which account for the modifications of the Zeeman energy splitting and the effective magnetic field angle due to the inclusion of SOI. For negligible SOI $\eta_{\text{so}} \ll 1$, $f_{\text{so}} \approx 1$ and $\vartheta \approx \theta_B$ for all \mathbf{B} field angles θ_B . in the very strong SOI regime, $\eta_{\text{so}} \geq 2$ and $f_{\text{so}} \approx \cos(\theta_B)$, and thus the effective \mathbf{B} field angle is strongly regulated as $\vartheta \approx 0$ for $\theta_B < \pi/2$ and $\vartheta \approx \pi$ for $\theta_B > \pi/2$, i.e., either parallel or antiparallel to the SOI vector. For an intermediate SOI strength, the behavior is between the above two limiting cases.

Further application of the non-degenerate perturbation theory in the rotated basis yields corrections from higher orbital states. Keeping terms only up to the first order in $\xi_Z \equiv E_Z/\hbar\Omega \ll 1$, we have

$$|\phi_{0\sigma}^{(1)}\rangle = |\phi_{0\sigma}^{(0p)}\rangle + \sum_{n=1}^{\infty} \chi_n \left[s_{\sigma}^n \cos(\frac{\vartheta}{2}) |\phi_{n\sigma}^{(0)}\rangle + s_{\sigma}^{n+1} \sin(\frac{\vartheta}{2}) |\phi_{n\sigma}^{(0)}\rangle \right]. \quad (\text{A13})$$

We have left out the normalization factor here for brevity. The mixing amplitudes with higher orbital states are given by $\chi_n = -\frac{1}{2}\xi_Z e^{-(x_0/x_{\text{SO}})^2} \sin(\theta_B) (\sqrt{2}ix_0/x_{\text{SO}})^n / (n\sqrt{n!})$, which are suppressed gradually as the orbital level n increases. Similar calculations can be carried out for higher orbital levels as well. This eventually gives rise to a complete basis of states, each with entangled spin and orbital parts. In this basis, Eq. (A5) is diagonal up to first order in ξ_Z , and its $n=0$ subspace defines the qubit Hamiltonian $H_Q = \frac{1}{2}\varepsilon_Z\sigma_c$. But the electric dipole term $\mathbf{E}(t) \cdot \mathbf{r}$ will not be diagonal due to nonzero matrix elements between neighboring orbital levels. This is the basis for the spin-orbit qubit and single qubit manipulations.

3. The double-dot basis

The only thing left unspecified in the Hamiltonian Eq. (A2) is the electro-static potential $V(\mathbf{r}) = V(x)$ of the DQD system. In the vicinity of the local minima $x = \pm d$, $V(x)$ is approximately harmonic. We shift the energy reference level such that $V(\mp d) = \pm\varepsilon/2$ and approximate the local harmonic potentials at $x = -d$ and $x = d$ by V_L and V_R . In general, the local harmonic frequencies could differ, but introducing different oscillator for each dot would be overcomplicated if only few lowest orbital levels are of interest. Here we bypass this issue by assuming that the dot frequencies are of a characteristic magnitude Ω . V_L and V_R are defined by translating the common potential $V_C = \frac{1}{2}m_e^*\Omega^2x^2$ to $V_{L/R} = \frac{1}{2}m_e^*\Omega^2(x \pm d)^2$ and shifting the energy by $\pm\varepsilon/2$. The differences from the exact local Taylor expansions are absorbed by ΔV_L and ΔV_R , respectively, such that the total DQD potential can be split as

$$V = V_L + \Delta V_L = V_R + \Delta V_R. \quad (\text{A14})$$

Assuming that the effective interdot barrier is much greater compared to the orbital spacing and the dots are well separated, the low energy eigenstates are mostly concentrated at the two single dots localied around $x = \pm d$. To capture those localized states, we consider translating a basis $\{|\phi_{n\sigma}^C\rangle\}$ for the V_C potential to the left and right dots,

$$|\phi_{n\sigma}^L\rangle = e^{ipd} |\phi_{n\sigma}^C\rangle, \quad |\phi_{n\sigma}^R\rangle = e^{-ipd} |\phi_{n\sigma}^C\rangle. \quad (\text{A15})$$

Further assuming that $\hbar\Omega \gg \varepsilon$ or E_Z , we can define a set of basis states O , ordered by increasing energy, by interleaving the two sets of basis states in Eq. (A15). O is over-complete and orthogonalization is required to make proper basis. Formulating a systematic orthogonalization procedure is not the focus of this work. As a low energy theory, we can truncate the basis to only consider the four lowest orbital states $O_{n=0}$. Given this basis does not involve higher orbital states anyway, it make little sense to use the fully perturbed states in Eq. (A13) either. But the degenerate perturbation required for breaking the Kramer degeneracy is necessary as it does not involve higher orbital states. We thus take the $\xi_Z \ll 1$ limit and consider the properly rotated ground orbital states at the center using Eq. (A10),

$$\begin{aligned} |\phi_{0\uparrow}^C\rangle &= \cos\frac{\vartheta}{2} e^{-ix/x_{\text{SO}}} |0\rangle|\uparrow\rangle + \sin\frac{\vartheta}{2} e^{+ix/x_{\text{SO}}} |0\rangle|\downarrow\rangle, \\ |\phi_{0\downarrow}^C\rangle &= \cos\frac{\vartheta}{2} e^{+ix/x_{\text{SO}}} |0\rangle|\downarrow\rangle - \sin\frac{\vartheta}{2} e^{-ix/x_{\text{SO}}} |0\rangle|\uparrow\rangle, \end{aligned} \quad (\text{A16})$$

where we follow the double-arrow convention to indicate entanglement in spin and orbital components, as opposed to single arrows for spin only.

To derive an orthonormal low-energy basis for the DQD system, we substitute Eq. (A16) into Eq. (A15) and calculate the state overlaps. States within the same dot are automatically orthonormal, since they are eigenstates of the local Hamiltonian, $\langle\phi_{\sigma}^L|\phi_{\sigma'}^L\rangle = \langle\phi_{\sigma}^R|\phi_{\sigma'}^R\rangle = \delta_{\sigma\sigma'}$. To calculate the interdot overlaps, we apply the vacuum expectation formula of displacement operators and find two distinct types of coefficients, i.e., the state overlaps between same spins and that between opposite spins,

$$s_d \equiv \langle\phi_{0\downarrow}^L|\phi_{0\downarrow}^R\rangle = \langle\phi_{0\uparrow}^L|\phi_{0\uparrow}^R\rangle^* = e^{-(d/x_0)^2} (\cos\gamma_{\text{SO}} - i\sin\gamma_{\text{SO}}\cos\vartheta), \quad (\text{A17})$$

$$s_x \equiv \langle\phi_{0\downarrow}^L|\phi_{0\uparrow}^R\rangle = \langle\phi_{0\uparrow}^L|\phi_{0\downarrow}^R\rangle = e^{-(d/x_0)^2} (-i\sin\gamma_{\text{SO}}\sin\vartheta). \quad (\text{A18})$$

To form an orthonormal DQD basis out of the local states, we label the four DQD basis states as $|\Phi_{L\downarrow}\rangle$, $|\Phi_{L\uparrow}\rangle$, $|\Phi_{R\downarrow}\rangle$ and $|\Phi_{R\uparrow}\rangle$, which are linear superpositions of the four local states,

$$\begin{aligned} |\Phi_{L\downarrow}\rangle &= c_{11}|\phi_{0\downarrow}^L\rangle + c_{12}|\phi_{0\uparrow}^L\rangle + c_{13}|\phi_{0\downarrow}^R\rangle + c_{14}|\phi_{0\uparrow}^R\rangle, \\ |\Phi_{L\uparrow}\rangle &= c_{21}|\phi_{0\downarrow}^L\rangle + c_{22}|\phi_{0\uparrow}^L\rangle + c_{23}|\phi_{0\downarrow}^R\rangle + c_{24}|\phi_{0\uparrow}^R\rangle, \\ |\Phi_{R\downarrow}\rangle &= c_{31}|\phi_{0\downarrow}^L\rangle + c_{32}|\phi_{0\uparrow}^L\rangle + c_{33}|\phi_{0\downarrow}^R\rangle + c_{34}|\phi_{0\uparrow}^R\rangle, \\ |\Phi_{R\uparrow}\rangle &= c_{41}|\phi_{0\downarrow}^L\rangle + c_{42}|\phi_{0\uparrow}^L\rangle + c_{43}|\phi_{0\downarrow}^R\rangle + c_{44}|\phi_{0\uparrow}^R\rangle. \end{aligned} \quad (\text{A19})$$

Applying the orthonormal condition for the basis states leads to a set of 10 independent equations. But there are in total 16 complex coefficients to solve. This indicates that there is a lot of freedom in choosing the basis states. For a representation that accurately depicting the low energy dynamics of the DQD system, we impose additional constrains out of locality and symmetry: The DQD basis states should capture the electron wave functions localized at a particular dot with a particular spin and should be symmetric with respect to the dot location and the spin direction. According to the locality principle, the DQD basis states should be considered as perturbations to the correspondingly local states. Here we choose the smallness factor to be $e^{-(d/x_0)^2}$. The premise that d/x_0 is large is in fact mandatory for well localized dot states. As the normalization factors can be added afterwards, we demand that $c_{ii} = 1$ with $c_{ij} = O(e^{-(d/x_0)^2})$ for $i \neq j$. Orthogonality yields a set of 6 independent complex constraints,

$$\sum_{i,j} c_{mi}^* c_{nj} \langle \phi_i | \phi_j \rangle = 0, \quad \text{for } n \neq m, \quad (\text{A20})$$

where we have used the shorthands ϕ_1, ϕ_2, ϕ_3 , and ϕ_4 for $\phi_{0\downarrow}^L, \phi_{0\uparrow}^L, \phi_{0\downarrow}^R$, and $\phi_{0\uparrow}^R$, respectively. According to the symmetry principle, transposing the dot or the spin labels should leave the amplitude of the respective coefficients invariant. This produces 9 real constrains,

$$\begin{aligned} |c_{12}| &= |c_{21}| = |c_{34}| = |c_{43}|, \\ |c_{13}| &= |c_{31}| = |c_{24}| = |c_{42}|, \\ |c_{14}| &= |c_{41}| = |c_{32}| = |c_{23}|. \end{aligned} \quad (\text{A21})$$

Still out of symmetry consideration, we further demand the normalization factors to be identical, leading to 3 additional real constraints,

$$\begin{aligned} \sum_{i,j} c_{1i}^* c_{1j} \langle \phi_i | \phi_j \rangle &= \sum_{i,j} c_{2i}^* c_{2j} \langle \phi_i | \phi_j \rangle \\ &= \sum_{i,j} c_{3i}^* c_{3j} \langle \phi_i | \phi_j \rangle = \sum_{i,j} c_{4i}^* c_{4j} \langle \phi_i | \phi_j \rangle. \end{aligned} \quad (\text{A22})$$

We now have 24 real constrains for 24 real unknowns. Therefore, these coefficients can be in principle fully solved, producing a unique DQD basis that is both localized and symmetric. The exact coefficients, however, are quite involved functions of s_d and s_x . For our treatments, it suffices to keep these expressions to the leading order in $e^{-(d/x_0)^2}$. Therefore, we make the shift $s_d \rightarrow \epsilon s_d$, $s_x \rightarrow \epsilon s_x$ and $c_{ij} \rightarrow \epsilon c_{ij} + \epsilon^2 d_{ij} + \dots$, $i \neq j$. Solving the constraints to the leading order, we have

$$\begin{aligned} c_{12} &= c_{21} = c_{34} = c_{43} = 0, \\ c_{13} &= c_{31}^* = c_{24}^* = c_{42} = -s_d^*/2, \\ c_{14} &= c_{41}^* = c_{23}^* = c_{32} = -s_x^*/2. \end{aligned} \quad (\text{A23})$$

These solutions are in fact good enough for all constraints to remain valid up to $O(\epsilon^2)$, Therefore we may write our DQD basis states as

$$\begin{aligned} |\Phi_{L\downarrow}\rangle &= |\phi_{0\downarrow}^L\rangle - \frac{1}{2}s_d^*|\phi_{0\downarrow}^R\rangle - \frac{1}{2}s_x^*|\phi_{0\uparrow}^R\rangle, \\ |\Phi_{L\uparrow}\rangle &= |\phi_{0\uparrow}^L\rangle - \frac{1}{2}s_d|\phi_{0\uparrow}^R\rangle - \frac{1}{2}s_x^*|\phi_{0\downarrow}^R\rangle, \\ |\Phi_{R\downarrow}\rangle &= |\phi_{0\downarrow}^R\rangle - \frac{1}{2}s_d|\phi_{0\downarrow}^L\rangle - \frac{1}{2}s_x|\phi_{0\uparrow}^L\rangle, \\ |\Phi_{R\uparrow}\rangle &= |\phi_{0\uparrow}^R\rangle - \frac{1}{2}s_d^*|\phi_{0\uparrow}^L\rangle - \frac{1}{2}s_x|\phi_{0\downarrow}^L\rangle. \end{aligned} \quad (\text{A24})$$

4. Low energy Hamiltonian and tunnelling coefficients

Equipped with the low energy basis, we proceed to derive the low energy Hamiltonian for the DQD system. In the field operator language, we may represent single-particle and two-particle interaction Hamiltonian by the creation a_μ^\dagger and annihilation operator a_μ for $|\Phi_\mu\rangle$ as

$$H_e = \sum_{\mu\nu} T_{\mu\nu} a_\mu^\dagger a_\nu, \quad H_{ee} = \frac{1}{2} \sum_{\mu\nu\rho\lambda} V_{\mu\nu\rho\lambda} a_\mu^\dagger a_\nu^\dagger a_\rho a_\lambda. \quad (\text{A25})$$

where the state indices in Eq. (A25) now include both the site and spin-orbit quantum numbers. The coefficients for the H_e are given by $T_{X\sigma, X'\sigma'} = \langle \Phi_{X\sigma} | \hat{H}_e | \Phi_{X'\sigma'} \rangle$, and there are 16 elements in total. Since the DQD basis states are linear combinations of the local dot states, these matrix elements are also linear combinations of the Hamiltonian matrix elements with respect to the local dot states, $\tilde{T}_{X\sigma, X'\sigma'} = \langle \phi_{X\sigma} | \hat{H}_e | \phi_{X'\sigma'} \rangle$, by the basis transformation given by Eq. (A24). According the Eq. (A14), we can decompose $H_e = H_L + \Delta V_L = H_R + \Delta V_R$, and calculate

$$\tilde{T} = \begin{pmatrix} \varepsilon_{L\downarrow} + v_- & 0 & s_d(\varepsilon_{R\downarrow} + v_0) & s_x(\varepsilon_{R\uparrow} + v_0) \\ 0 & \varepsilon_{L\uparrow} + v_- & s_x(\varepsilon_{R\downarrow} + v_0) & s_d^*(\varepsilon_{R\uparrow} + v_0) \\ s_d^*(\varepsilon_{R\downarrow} + v_0^*) & s_x^*(\varepsilon_{R\downarrow} + v_0^*) & \varepsilon_{R\downarrow} + v_+ & 0 \\ s_x^*(\varepsilon_{R\uparrow} + v_0^*) & s_d(\varepsilon_{R\uparrow} + v_0^*) & 0 & \varepsilon_{R\uparrow} + v_+ \end{pmatrix} \quad (\text{A26})$$

where $\varepsilon_{L/R, \sigma} = \pm\varepsilon + s_\sigma \frac{1}{2} \varepsilon_{L/R, Z}$ is the energy of the local Hamiltonian $H_{L/R}$, while

$$\begin{aligned} v_- &\equiv \langle 0 | e^{-ipd} \Delta V_L e^{ipd} | 0 \rangle = \langle 0 | \Delta V_L(x-d) | 0 \rangle, \\ v_+ &\equiv \langle 0 | e^{ipd} \Delta V_R e^{-ipd} | 0 \rangle = \langle 0 | \Delta V_R(x+d) | 0 \rangle, \end{aligned} \quad (\text{A27})$$

are the energy corrections due to the existence of the other dot, and finally,

$$v_0 \equiv \frac{\langle 0 | e^{-ipd} \Delta V_R e^{-ipd} | 0 \rangle}{\langle 0 | e^{-2ipd} | 0 \rangle} = \langle 0 | \Delta V_R(x) | 0 \rangle, \quad (\text{A28})$$

where we have used the Wick's theorem to simplify the vacuum expectations (see Appendix A 4 a). Since $\Delta V_{L/R}$ is by definition close to zero in the vicinity of $x = \mp d$, the values of v_- and v_+ are typically much smaller than other energy scales. On the other hand, v_0 is related to barrier of the DQD system. Specifically, for $d \gg x_0$, one can approximate

$$v_0 \approx V(0) - V(d) - \frac{1}{2} m_e^* \Omega^2 d^2. \quad (\text{A29})$$

As illustrated in Fig. 6, the parabolically shaped V_R will tend to overestimate the DQD potential V at $x = 0$. Therefore v_0 is negative and its magnitude is typically much greater than other energy scales such as the orbital detuning and the Zeeman energy. Furthermore, increasing the barrier height V_{ba} will decrease $|v_0|$, thus decreasing the tunneling amplitude. This is consistent with typical observations.

Transformating to the DQD basis and keep the terms up to the first order of the smallness factor $e^{-(d/x_0)^2}$, we find,

$$T = \begin{pmatrix} \varepsilon_{L\downarrow} + v_- & 0 & t_\downarrow & s_\downarrow \\ 0 & \varepsilon_{L\uparrow} + v_- & s_\uparrow & t_\uparrow \\ t_\downarrow^* & s_\uparrow^* & \varepsilon_{R\downarrow} + v_+ & 0 \\ s_\downarrow^* & t_\uparrow^* & 0 & \varepsilon_{R\uparrow} + v_+ \end{pmatrix}, \quad (\text{A30})$$

where we introduce the tunneling coefficients

$$\begin{aligned} t_\downarrow &= s_d \left(\frac{1}{2} \varepsilon_{R\downarrow} - \frac{1}{2} \varepsilon_{L\downarrow} + v_0 - \frac{1}{2} v_- - \frac{1}{2} v_+ \right), \\ t_\uparrow &= s_d^* \left(\frac{1}{2} \varepsilon_{R\uparrow} - \frac{1}{2} \varepsilon_{L\uparrow} + v_0 - \frac{1}{2} v_- - \frac{1}{2} v_+ \right), \\ s_\downarrow &= s_x \left(\frac{1}{2} \varepsilon_{R\uparrow} - \frac{1}{2} \varepsilon_{L\downarrow} + v_0 - \frac{1}{2} v_- - \frac{1}{2} v_+ \right), \\ s_\uparrow &= s_x \left(\frac{1}{2} \varepsilon_{R\downarrow} - \frac{1}{2} \varepsilon_{L\uparrow} + v_0 - \frac{1}{2} v_- - \frac{1}{2} v_+ \right). \end{aligned} \quad (\text{A31})$$

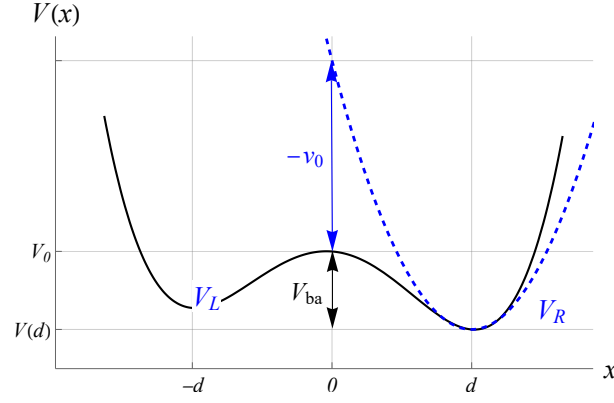


FIG. 6. The v_0 term as determined by the potential profile

The dot Hamiltonian H_d is defined according to the diagonal part of the T tensor. We may redefine the effective chemical potentials to $\tilde{\varepsilon}_{L\sigma} = \varepsilon_{L\sigma} + v_-$ and $\tilde{\varepsilon}_{R\sigma} = \varepsilon_{L\sigma} + v_+$; or, as argued earlier, simply neglect the v_{\pm} terms since they are very small. Since shifting the global energy level has trivial influence on the qubit dynamics, We can reset $\tilde{\varepsilon}_L + \tilde{\varepsilon}_R = 0$ and define detuning $\varepsilon = \tilde{\varepsilon}_L - \tilde{\varepsilon}_R$. by

$$\hat{H}_d = \sum_{\sigma=\uparrow,\downarrow} \frac{1}{2}(\varepsilon + s_{\sigma}\varepsilon_{Z,L})n_{L\sigma} + \frac{1}{2}(-\varepsilon + s_{\sigma}\varepsilon_{Z,R})n_{R\sigma} \quad (\text{A32})$$

The Zeeman splitting energy can be further rearranged into the average splitting $\varepsilon_Z = (\varepsilon_{Z,L} + \varepsilon_{Z,R})/2$ and the energy difference $\delta\varepsilon_Z = (\varepsilon_{Z,L} - \varepsilon_{Z,R})$.

The tunneling Hamiltonian H_t is the off-diagonal part of the T tensor. In principle, there are mechanisms involved: spin-preserved and spin-flipped tunneling, in addition to on-site spin flipping. If there is no oscillatory electric field, on-site flipping term is absent and we have,

$$H_t = \sum_{\sigma=\uparrow,\downarrow} (t_{\sigma}a_{L\sigma}^{\dagger}a_{R\sigma} + s_{\sigma}a_{L\sigma}^{\dagger}a_{R\bar{\sigma}} + h.c.), \quad (\text{A33})$$

where spin-dependent tunneling coefficients are given by Eq. (A31). Calculating these coefficients requires knowledge of the full potential profile, but the details of the potential contributes trivially to the the gate dynamics by v_0, v_- and v_+ . In the presence of the barrier term v_0 , the Zeeman energy differences in the parentheses of Eq. (A31) can be safely ignored. Combining with Eq. (A17), we can define a common tunneling strength $t_0 \propto e^{-(d/x_0)^2}$ for the spin-conserved tunneling t and spin-flipped tunneling s , which are related by

$$t \equiv t_{\downarrow} = t_{\uparrow}^* = t_0 \left[\cos(\gamma_{SO}) - i \sin(\gamma_{SO}) \cos(\vartheta) \right], \quad (\text{A34})$$

$$s \equiv s_{\downarrow} = s_{\uparrow} = t_0 \left[-i \sin(\gamma_{SO}) \sin(\vartheta) \right]. \quad (\text{A35})$$

Finally, the electron interaction energy involves in many terms and can also contribute to the exchange interaction. This is known as direct exchange and it mainly affects doubly occupied sites. This differs from the kinetic exchange that arises from H_t . Here we only consider leading order effect where all terms in the V tensor are ignored and only on-site Coulomb repulsion is considered. This can be summarized as

$$H_C = \sum_{j=L,R} \sum_{\sigma=\uparrow,\downarrow} \frac{U}{2} a_{j\sigma}^{\dagger} a_{j\bar{\sigma}}^{\dagger} a_{j\bar{\sigma}} a_{j\sigma} \quad (\text{A36})$$

a. Deriving the electro-static potential terms

We have derived the expression of v_0 in the following manner. Define $\alpha_d = d/\sqrt{2}x_0$, then

$$e^{-ipd}|0\rangle = D(\alpha_d)|0\rangle = |\alpha_d\rangle, \quad (\text{A37})$$

where $D(\alpha)$ is the displacement operator and $|\alpha\rangle$ represents a coherent state. The smallness factor considered in our problem is essentially

$$\langle 0|D(\alpha_d)D(\alpha_d)|0\rangle = \langle -\alpha_d|\alpha_d\rangle = e^{-(d/x_0)^2}, \quad (\text{A38})$$

and we can rewrite v_0 as

$$v_0 = \frac{\langle -\alpha_d|\Delta V_R|\alpha_d\rangle}{\langle -\alpha_d|\alpha_d\rangle}. \quad (\text{A39})$$

To calculate the numerator, we consider expanding it as a power series of x . This would require calculation of the matrix element:

$$\langle -\alpha_d|x^n|\alpha_d\rangle = \left(\frac{x_0}{\sqrt{2}}\right)^n \langle -\alpha_d|(a + a^\dagger)^n|\alpha_d\rangle \quad (\text{A40})$$

Expanding the n th power will lead to a summation of all possible sequences of n field operators. Using Wick's theorem, any field operator sequence can be converted to the normal order sequence plus all possible normal ordered contractions. Therefore,

$$\begin{aligned} (a + a^\dagger)^n &= \sum_{k=0}^n \binom{n}{k} (a^\dagger)^k a^{n-k} + \sum_{\text{1-contr.}} \sum_{k=0}^{n-2} \binom{n-2}{k} (a^\dagger)^k a^{n-2-k} \\ &+ \sum_{\text{2-contr.}} \sum_{k=0}^{n-4} \binom{n-4}{k} (a^\dagger)^k a^{n-4-k} + \dots \end{aligned} \quad (\text{A41})$$

Using the property $a|\alpha_d\rangle = \alpha_d|\alpha_d\rangle$ and its conjugate variant, we have

$$\langle -\alpha_d|\sum_{k=0}^m \binom{m}{k} (a^\dagger)^k a^{m-k}|\alpha_d\rangle = \sum_{k=0}^m \binom{m}{k} (-\alpha_d)^k \alpha_d^{m-k} = 0. \quad (\text{A42})$$

The only nonzero terms would be the fully contracted terms, which requires n to be even and there are $(n-1)!!$ possible contractions. Apart from the factor of $\langle -\alpha_d|\alpha_d\rangle$, this result coincides with the vacuum expectation value. Hence

$$v_0 = \langle 0|\Delta V_R(x)|0\rangle. \quad (\text{A43})$$

5. Hamiltonian in the computational space

In order to derive the effective exchange Hamiltonian, we expand the system Hamiltonian in the six low energy two-electron spin basis that consists of 4 states in the $(1, 1)$ configuration and the singlet state $S(2, 0)$ and $S(0, 2)$. Each of these basis are antisymmetric two-electron wave functions. The tunneling Hamiltonian, for example, acts on the $|\downarrow\uparrow\rangle$ by

$$\begin{aligned} H_t|\downarrow\uparrow\rangle &= H_t \frac{1}{\sqrt{2}} (|\Phi_{L\downarrow}\rangle|\Phi_{R\uparrow}\rangle - |\Phi_{R\uparrow}\rangle|\Phi_{L\downarrow}\rangle) \\ &= -t^*|S(2, 0)\rangle - t^*|S(0, 2)\rangle. \end{aligned} \quad (\text{A44})$$

Using similar calculations, we can represent the low energy Hamiltonian as

$$H_6 \hat{=} \begin{pmatrix} \varepsilon_Z & 0 & 0 & 0 & s^* & -s \\ 0 & \frac{1}{2}\delta\varepsilon_Z & 0 & 0 & t^* & t^* \\ 0 & 0 & -\frac{1}{2}\delta\varepsilon_Z & 0 & -t & -t \\ 0 & 0 & 0 & -\varepsilon_Z & -s^* & s \\ s & t & -t^* & -s & U - \varepsilon & 0 \\ -s^* & t & -t^* & s^* & 0 & U + \varepsilon \end{pmatrix}, \quad (\text{A45})$$

under the basis $\{|\uparrow\uparrow\rangle, |\uparrow\downarrow\rangle, |\downarrow\uparrow\rangle, |\downarrow\downarrow\rangle, |S(2,0)\rangle, |S(0,2)\rangle\}$. Assuming that the on-site Coulomb energy is much larger than the tunneling energy: $U \gg t_0$, we would have three different energy blocks—(1, 1), (0, 2), (2, 0) with weak coupling. The DC gates work exclusively in the (1, 1) charge configuration. To find the influence of other energy levels on the (1, 1) space, we project H_6 in to four (1, 1) states space using the Schrieffer-Wolff transformation $e^S H_6 e^{-S}$. Define the diagonal and off-diagonal part of H_6 as H_{60} and H_{61} , the transformation matrix S must satisfy the condition $[H_{60}, S] = H_{61}$. And the effective Hamiltonian in the (1, 1) charge configuration can be approximate with

$$H = \mathcal{P}_{(1,1)} \left(H_{60} + \frac{1}{2}[S, H_{61}] \right) + O((t_0/U)^4). \quad (\text{A46})$$

Since H_{60} is diagonal, S can be explicitly found by,

$$S_{ii} = 0, \quad S_{ij} = \frac{(H_{61})_{ij}}{(H_{60})_{ii} - (H_{60})_{jj}} \quad (i \neq j). \quad (\text{A47})$$

Substituting into Eq. (A46), we can write the resulting effective Hamiltonian as

$$H = H_0 + H_{\text{ex}}, \quad (\text{A48})$$

where,

$$H_0 \hat{=} \text{diag}(\varepsilon_Z, \frac{1}{2}\delta\varepsilon_Z, -\frac{1}{2}\delta\varepsilon_Z, -\varepsilon_Z) \quad (\text{A49})$$

is a diagonal matrix that arises solely from the local Zeeman field for each dot. H_{ex} is responsible for the exchange coupling, explicitly given by its (i, j) th element,

$$(H_{\text{ex}})_{ij} = -2(\mathbf{j}_i + \mathbf{j}_j)\boldsymbol{\xi}_i\boldsymbol{\xi}_j^*, \quad (\text{A50})$$

where we introduce vectors $\mathbf{j} = (j_-^a, j_-^b, j_+^b, j_+^a)^T$, and $\boldsymbol{\xi} = 1/(\sqrt{2}t_0)(s^*, t^*, -t, s)^T$, with

$$\begin{aligned} j_{\pm}^a &= \frac{t_0^2}{2} \left(\frac{1}{U \pm \varepsilon_Z - \varepsilon} + \frac{1}{U \pm \varepsilon_Z + \varepsilon} \right), \\ j_{\pm}^b &= \frac{t_0^2}{2} \left(\frac{1}{U \pm \delta\varepsilon_Z - \varepsilon} + \frac{1}{U \pm \delta\varepsilon_Z + \varepsilon} \right). \end{aligned} \quad (\text{A51})$$

By assumption $U \gg \varepsilon_Z, \delta\varepsilon_Z$, we can make the approximation

$$j_{\pm}^a \approx j_{\pm}^b \approx \frac{t_0^2}{2} \left(\frac{1}{U - \varepsilon} + \frac{1}{U + \varepsilon} \right) \equiv \frac{J}{4}. \quad (\text{A52})$$

Due to the form $\boldsymbol{\xi}$ is defined, we can define normalized state $|\xi\rangle$ as the entangled two-qubit state

$$|\xi\rangle = \frac{1}{\sqrt{2}} (|\uparrow\rangle|\nearrow\rangle - |\downarrow\rangle|\swarrow\rangle), \quad (\text{A53})$$

where,

$$\begin{cases} |\nearrow\rangle = \tilde{s}^*|\uparrow\rangle + \tilde{t}^*|\downarrow\rangle, \\ |\swarrow\rangle = \tilde{t}|\uparrow\rangle - \tilde{s}|\downarrow\rangle \end{cases} \quad (\text{A54})$$

are a pair of orthogonal spin states with normalized coefficients $|\tilde{s}|^2 + |\tilde{t}|^2 = 1$ given by $\tilde{s} = s/t_0$ and $\tilde{t} = t/t_0$. This leads to the final expression for the exchange coupling Hamiltonian

$$H_{\text{ex}} = -J|\xi\rangle\langle\xi|, \quad (\text{A55})$$

a very compact outcome.

Appendix B: Perturbative results for the CZ gate

Let us calculate the eigenenergies of H to the second order. Using non-degenerate perturbation theory, we obtain

$$\begin{aligned}
\delta E_1 &\approx -\left(\frac{J}{\varepsilon_Z}\right) \frac{|\tilde{s}|^2}{2} + \left(\frac{J}{\varepsilon_Z}\right)^2 \left(\frac{|\tilde{s}|^4}{8} + \frac{|\tilde{s}|^2|\tilde{t}|^2}{4+2\delta} + \frac{J^2|\tilde{s}|^2|\tilde{t}|^2}{4-2\delta} \right), \\
\delta E_2 &\approx -\left(\frac{J}{\varepsilon_Z}\right) \frac{|\tilde{t}|^2}{2} + \left(\frac{J}{\varepsilon_Z}\right)^2 \left(\frac{|\tilde{t}|^4}{4\delta} + \frac{|\tilde{s}|^2|\tilde{t}|^2}{4+2\delta} - \frac{J^2|\tilde{s}|^2|\tilde{t}|^2}{4-2\delta} \right), \\
\delta E_3 &\approx -\left(\frac{J}{\varepsilon_Z}\right) \frac{|\tilde{t}|^2}{2} + \left(\frac{J}{\varepsilon_Z}\right)^2 \left(-\frac{|\tilde{t}|^4}{4\delta} - \frac{|\tilde{s}|^2|\tilde{t}|^2}{4+2\delta} + \frac{J^2|\tilde{s}|^2|\tilde{t}|^2}{4-2\delta} \right), \\
\delta E_4 &\approx -\left(\frac{J}{\varepsilon_Z}\right) \frac{|\tilde{s}|^2}{2} + \left(\frac{J}{\varepsilon_Z}\right)^2 \left(-\frac{|\tilde{s}|^4}{8} - \frac{|\tilde{s}|^2|\tilde{t}|^2}{4+2\delta} - \frac{J^2|\tilde{s}|^2|\tilde{t}|^2}{4-2\delta} \right),
\end{aligned} \tag{B1}$$

where $\delta \equiv \delta\varepsilon_Z/\varepsilon_Z$. The first and second order energy corrections all lead to the evolution time in Eq. (14). Combined with the phase-matching conditions $\phi_0 = -\delta E_1\tau_{CZ}$, $\phi_0 + \phi_R = -\delta E_2\tau_{CZ}$ and $\phi_0 + \phi_L = -\delta E_3\tau_{CZ}$, the corresponding local phase corrections are found to be

$$\begin{aligned}
\phi_L &= \pm \frac{\pi}{2} \left[1 + \frac{J}{4\varepsilon_Z} \frac{2(2+\delta)|\tilde{t}|^4 + \delta(2+\delta)|\tilde{s}|^4 + 8\delta|\tilde{s}|^2|\tilde{t}|^2}{4\delta(2+\delta)(|\tilde{t}|^2 - |\tilde{s}|^2)} \right], \\
\phi_R &= \pm \frac{\pi}{2} \left[1 - \frac{J}{4\varepsilon_Z} \frac{2(2-\delta)|\tilde{t}|^4 - \delta(2-\delta)|\tilde{s}|^4 - 8\delta|\tilde{s}|^2|\tilde{t}|^2}{4\delta(2-\delta)(|\tilde{t}|^2 - |\tilde{s}|^2)} \right],
\end{aligned} \tag{B2}$$

where the \pm signs in the front is '+' when $|\tilde{t}| > |\tilde{s}|$ and '-' when $|\tilde{t}| < |\tilde{s}|$.

The global and local phase corrections define a phase correction vector $\vec{\phi}_{\text{corr}} = \tau_{CZ}(\delta E_1, \delta E_2, \delta E_3, \delta E_2 + \delta E_3 - \delta E_1)$. Carrying out the phase corrections to $\tilde{U}(\tau_{CZ})$ produces the phase-corrected gate $\tilde{U}_c(\tau_{CZ}) = e^{i\vec{\phi}_{\text{corr}}} \tilde{U}(\tau_{CZ})$, whose diagonal elements are given by

$$\langle n | \tilde{U}_c(\tau_{CZ}) | n \rangle = \sum_m |\langle n | m' \rangle|^2 \exp[-i(E'_m - E_n^{(0)})\tau_{CZ} + i\vec{\phi}_{\text{corr},n}] \equiv \sum_m |\langle n | m' \rangle|^2 \Phi_{n,m}, \tag{B3}$$

where the phase matrix $\Phi_{n,m}$ introduced above is given by

$$\Phi_{n,m} = \begin{pmatrix} 1 & e^{-i(1-\delta/2)\tau_{CZ}} & e^{-i(1+\delta/2)\tau_{CZ}} & e^{-i2\tau_{CZ}} \\ e^{i(1-\delta/2)\tau_{CZ}} & 1 & e^{-i\delta\tau_{CZ}} & e^{-i(1+\delta/2)\tau_{CZ}} \\ e^{i(1+\delta/2)\tau_{CZ}} & e^{i\delta\tau_{CZ}} & 1 & e^{-i(1-\delta/2)\tau_{CZ}} \\ -e^{i2\tau_{CZ}} & -e^{i(1+\delta/2)\tau_{CZ}} & -e^{i(1-\delta/2)\tau_{CZ}} & -1 \end{pmatrix}. \tag{B4}$$

The perturbed eigenstates can be calculated as,

$$\begin{aligned}
|1'\rangle &= \frac{1}{\sqrt{N_1}} \left[|1\rangle + \frac{J}{\varepsilon_Z} \left(-\frac{st^*}{2-\delta} |2\rangle + \frac{st}{2+\delta} |3\rangle - \frac{s^2}{4} |4\rangle \right) + O\left(\frac{J}{\varepsilon_Z}\right)^2 \right] \\
|2'\rangle &= \frac{1}{\sqrt{N_2}} \left[|2\rangle + \frac{J}{\varepsilon_Z} \left(\frac{s^*t}{2-\delta} |1\rangle - \frac{st}{2+\delta} |4\rangle + \frac{t^2}{2\delta} |3\rangle \right) + O\left(\frac{J}{\varepsilon_Z}\right)^2 \right] \\
|3'\rangle &= \frac{1}{\sqrt{N_3}} \left[|3\rangle + \frac{J}{\varepsilon_Z} \left(\frac{st^*}{2-\delta} |4\rangle - \frac{s^*t^*}{2+\delta} |1\rangle - \frac{(t^*)^2}{2\delta} |2\rangle \right) + O\left(\frac{J}{\varepsilon_Z}\right)^2 \right] \\
|4'\rangle &= \frac{1}{\sqrt{N_4}} \left[|4\rangle + \frac{J}{\varepsilon_Z} \left(-\frac{s^*t}{2-\delta} |3\rangle + \frac{s^*t^*}{2+\delta} |2\rangle + \frac{(s^*)^2}{4} |1\rangle \right) + O\left(\frac{J}{\varepsilon_Z}\right)^2 \right],
\end{aligned} \tag{B5}$$

where the normalization factors N_1 , N_2 , N_3 and N_4 can be determined up to $O(J/\varepsilon_Z)^2$ from the above. The gate infidelity is calculated by taking the trace product of $\tilde{U}_c(\tau_{CZ})$ with the CZ gate, which only involves in the diagonal elements specified above. After substituting the evolution time and phase corrections, we can calculate, up

to $O(J/\varepsilon_Z)^2$, the gate infidelity as

$$\begin{aligned} \text{InF}_{\text{CZ}} = \frac{1}{20} \left(\frac{J}{\varepsilon_Z} \right)^2 & \left(|\tilde{s}|^4 [1 - \cos(2\varepsilon_Z \tau_{\text{CZ}})] + \frac{4|\tilde{t}|^4}{\delta^2} [1 - \cos(\delta\varepsilon_Z \tau_{\text{CZ}})] \right. \\ & \left. + \frac{32|\tilde{s}|^2|\tilde{t}|^2}{(2-\delta)^2} [1 - \cos(\varepsilon_Z(1-\frac{\delta}{2})\tau_{\text{CZ}})] + \frac{32|\tilde{s}|^2|\tilde{t}|^2}{(2+\delta)^2} [1 - \cos(\varepsilon_Z(1+\frac{\delta}{2})\tau_{\text{CZ}})] \right) + O\left(\frac{J}{\varepsilon_Z}\right)^3. \end{aligned} \quad (\text{B6})$$

This infidelity expression depends on the evolution time τ_{CZ} through the cosine terms. We can further discard the oscillatory cosine parts and bound

$$\text{InF}_{\text{CZ}} \lesssim \frac{1}{10} \left(\frac{J}{\varepsilon_Z} \right)^2 \left[|\tilde{s}|^4 + \frac{4|\tilde{t}|^4}{\delta^2} + \frac{64(4+\delta^2)}{(4-\delta^2)^2} |\tilde{s}|^2 |\tilde{t}|^2 \right]. \quad (\text{B7})$$